NARROW BAND STATE OF CHARGE CONTROLLED ENERGY MANAGEMENT SYSTEM FOR HYBRID RTG CRANES BASED ON STATE MACHINE CONTROLLER

Sheron Ruchiranga Anton Bolonne

178096B

Degree of Master of Science by Research

Department of Electrical Engineering

University of Moratuwa

Sri Lanka

May 2019

NARROW BAND STATE OF CHARGE CONTROLLED ENERGY MANAGEMENT SYSTEM FOR HYBRID RTG CRANES BASED ON STATE MACHINE CONTROLLER

Sheron Ruchiranga Anton Bolonne

178096B

Thesis submitted in fulfillment of the requirements for the degree of Master of Science by Research

Department of Electrical Engineering

University of Moratuwa

Sri Lanka

May 2019

DECLARATION

I declare that this is my own work and this thesis does not incorporate without acknowledgement any material previously submitted for a Degree or Diploma in any other University or institute of higher learning and to the best of my knowledge and belief it does not contain any material previously published or written by another person except where the acknowledgement is made in the text.

Also, I hereby grant to University of Moratuwa the non-exclusive right to reproduce and distribute my thesis, in whole or in part in print, electronic or other medium. I retain the right to use this content in whole or part in future works (such as articles or books).

Signature: Date:

The above candidate has carried out research for the Masters/MPhil/PhD thesis / Dissertation under my supervision.

Signature of the supervisor: Date

ABSTRACT

This research evaluates possibility of using a new hybrid system based on variable speed diesel generator (VSDG), Li-ion battery bank and supercapacitor bank (SC) for a rubber tire gantry crane (RTGC) used in container terminals. Existing commercial hybrid systems face difficulties producing high efficiencies, higher life span and lower initial investment cost due to inheriting characteristics of batteries and supercapacitors. In the proposed power system, a variable speed diesel generator act as the principal energy source, while a Li-ion battery bank and SC bank act as an energy storage system. The battery supports the diesel generator during steady demand and further, it absorbs a part of energy during regeneration. The energy management strategy controls the power flow from different sources while maintaining battery SOC level within a narrow band. Unlike most battery systems, this narrow band operation of battery system increases its life span while reducing capacity fade. The originality of this study can be emphasized from this narrow band SOC control technique. Simulation results for real operational load cycles are presented showing a stable system operating under defined current limits which can enhance lifetime of battery system and increase fuel saving by downsizing 400kW constant speed diesel generator to 200kW VSDG.

Keywords— RTG cranes, Hybrid energy storage, Energy management, narrow SOC band

ACKNOWLEDGEMENT

CONTENTS

LIST OF FIGURES

LIST OF TABLES

LIST OF ABBREVIATIONS

STS   : Ship to Shore

AGV : Automated Guided Vehicles

RTG : Rubber Tire Gantry

RMG : Rail Mounted Gantry

SWL : Standard Weight Limit

ICE   : Internal Combustion Engine

SC   : Supercapacitor

EMS : Energy Management System

RTGC : Rubber Tire Gantry Crane

DG   : Diesel Generator

VSDG : Variable Speed Diesel Generator

AC   : Alternating Current

DC   : Direct Current

BSFC : Brake Specific Fuel Consumption

CCM : Controlled Current Mode

CVM : Constant Voltage Mode

OCV : Open Circuit Voltage

1. INTRODUCTION

In a global economy, no country is self-sufficient that every nation is associate with specific flows of goods, information and people. Transportation of goods between countries and continents had created an international trade century ago which have laid foundations for the present transport and logistic system which plays an important part in international trade. Chain of sea-ports, ships and terminals have become the most efficient way of transport in logistics. This chapter serves as a general introduction for the rest of the thesis. Section 1.1 starts with some background information about container cranes and hybrid rubber tire gantry cranes. Section 1.2 describe the problem that is going to be addressed in thesis and finally Section 1.3 highlight the structure of the rest of the thesis.

1.1. Container Shipping

Container shipping does a vital role in transport and logistic sector. Day by day thousands of containers are joined to global container fleet to fulfill the increasing demand. 1950s first shipping container was introduced to reduce the service time for loading and unloading cargo. This technology cuts off the service time from weeks to few hours as what we experience today. Global trading is making over 200 million trips per year between seaports and container terminals such as Port of Colombo in Figure 1.1. In terms of imports and exports, international container trade is believed to account for roughly 60% of all world seaborne trade, that is valued at around twelve trillion U.S. dollars in 2017 [1].

There are few categories of cranes available inside container terminals to move containers from ships to shore and within the yard, see Figure 1.2. There are ship-to-shore cranes (STS), that use to unload and load containers from ships as soon as possible where multiple cranes working for single ship. Then the containers are transported to stacking yard. This operation is carried out by the terminal tractors, automated guided vehicles (AGVs) or saddle carriers. Finally, containers are stacked in storage yard before they are transported on land by trucks or freight trains. In some terminals this stacking is carried out by saddle carriers but use of rail mounted gantry cranes and rubber tire gantry (RTG) cranes is the popular method. This research focuses on RTG cranes which is much more flexible in yard horizontal movement

compared to rail mounted gantry (RMG) cranes which are mounted on rails and power by an automated cable reel.

Figure 1.1 : Port of Colombo, South Asia Gateway Terminals (Pvt) Ltd.

(a) STS Crane

(b) RTG Crane

(c) RMG Crane

(d) Straddle Carrier

(e) AGV

(f) Terminal Tractor

Figure 1.2 : Container handling equipment

The RTG cranes can travel on several lanes of stacked containers and move 20ft and 40ft containers weighting up to 65t. There are two-wheel configurations, 8-wheel and 16-wheel models where typical standard weight limit (SWL) of 8-wheel configuration is 40t while SWL of 16-wheel can be varied from 40t to 65t. These

2

cranes have rubber tires that enable them to travel through container storage blocks and switch to different container storage block easily. This is an advantage over rail mounted gantry crane which is always restricted to single container storage lane. These cranes are driven by an operator inside the control cabin which is placed underneath the trolley.
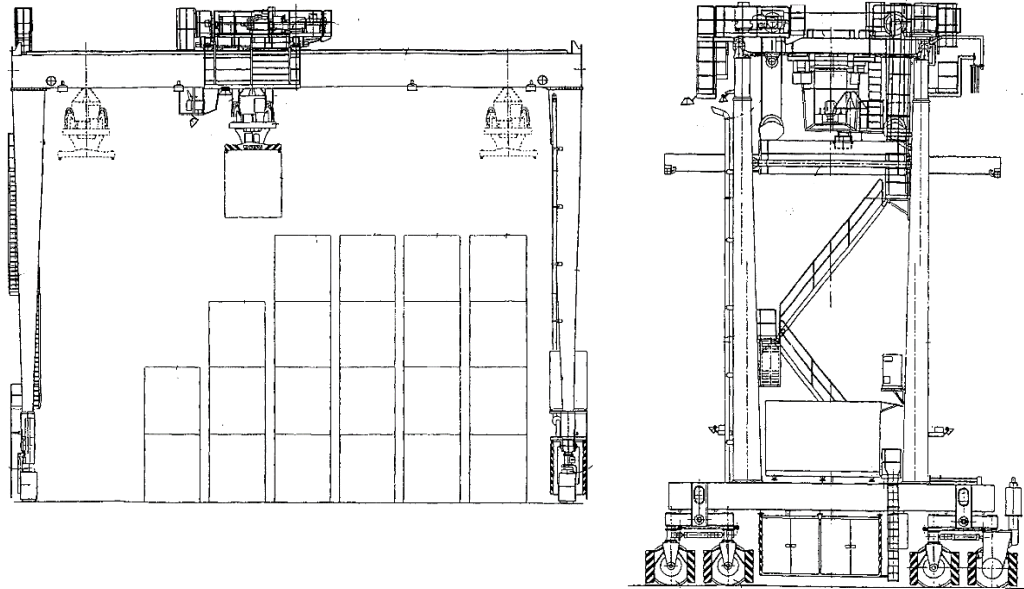
Figure 1.3 : Front view and side view of a RTG crane

Liebherr cranes, Kono cranes, Kalmar, Kunez, Paceco-Mitusi and Shanghai Zhenhua Heavy Industries Co. (formerly ZPMC) are some popular manufacturers for RTG cranes. Presently vast majority of cranes are manufactured by Shanghai Zhenhua Heavy Industries in China. Electrical systems of these cranes manufactured by ZPMC are sub-contracted to different parties such as Siemens, ABB, Fuji electric, Yaskawa, Danfoss and Emerson etc.

1.2. Hybrid RTG cranes

Hybrid system are becoming popular today, where most of the newly designed vehicles on production   have some sort of fuel saving technology, either engine start stop or hybrid. A moving mass has kinetic energy that can be recovered during descending downhill or deceleration. Energy recovery can be done in several energy forms such as, electrical energy, mechanical energy, compressed air or inform of hydraulic. The energy can be effectively utilized by recovering this energy as electrical energy compared to other forms.

Two hybrid structures can be found in hybrid vehicle drivetrains. They are series hybrid system and parallel hybrid system. Parallel hybrid systems have both an internal combustion engine (ICE) and an electric motor that can both individually drive the system (vehicle) or both can jointly supply power requirement. The axles of ICE and generator are coupled to a gearbox connecting through a clutch or a flywheel. The output shaft of the gearbox coupled to drive system.

Electrical transmission has been developed as an alternative to conventional mechanical transmission from 1903 [2]. Mechanical transmission imposes many disadvantages such as weight, bulk, noise, cost and maintenance. In series hybrid systems internal combustion engine turns a generator which is not mechanically connected to driving wheels. This series hybrid structure is highly popular in traction applications and marine systems, such as diesel electric locomotives, dump trucks and hybrid ships.

Hauling containers is more likely to be a hybrid activity due to the high amount of potential energy that can be recovered during lowering phase of containers. Energy savings and low emissions of CO_2 have made hybrid RTG cranes popular and ecofriendly. RTG cranes are hybridized with different configurations of energy sources. Battery banks, super-capacitor (SC) banks and fly-wheels are currently used as energy storage systems for RTG cranes. Commercial hybrid systems are available with battery systems and supercapacitor systems which record fuel savings upto 50% [3]. Almost all hybrid systems adopt series hybrid architecture due to the present system configuration of the RTG cranes.

1.3. Problem Statement

1.3.1. Main Thesis Goal

With the upcoming trend on "green" terminal concept, most of the RTG crane manufactories try to develop hybrid RTG cranes and to stay in front of their business. This leads to the prime problem that is discussed in this thesis:

How can an energy management system and hybrid storage system will enhance the life time of the energy storage system and maintain the fuel efficiency that is promised by the existing hybrid RTG crane systems?

A fuel saving crane with low performance (slow speeds on hoisting, trolleying and travelling) is not interested by terminal operators, whose top concern is to maximize the container handling output. Therefore, possible solutions are restraint by the performance of cranes cannot be de-rated.

1.3.2. Objectives

Three objectives are mainly focused during the research. These objectives cover broad area starting from selection of energy storage devices for hybrid storage system to development of energy management strategy and its validation through simulations. Objectives are lined as follows,

1. Define the paraments of a hybrid energy storage device and its characteristics.
2. Identify the control parameters of the system and develop the controller.
3. Develop an energy management strategy to utilize the propose the hybrid energy storage system and the generator set.

1.4. Outline

The contents of the rest of the thesis are structured as the same way as the three objectives. In the first two chapters, RTG crane structure is discussed. Chapter 2 explains the power consumption of RTG cranes, a system that simulates the power demand during operation. Chapter 3 deals with hybrid energy storage system where sizing of energy storage components and mathematical modeling of energy storage system is carried out. This model serves as the simulation model for energy storage components for the design discussed throughout the thesis.

In Chapter 4, the system integration of the hybrid energy storage system is explained which corresponds to the second objective. The chapter starts with a brief introduction to the existing systems in conventional RTG and experimental hybrid RTG cranes.

In Chapter 5, the actual design of the strategy is explained which relates to third objective. The simulation results of the energy management strategy are highlighted with its energy savings. Finally, Chapter 6 draws conclusions about the success of the project and present some recommendations about future improvement.

2. DEMAND MODEL

The initial step in the design process of hybrid system is the understanding how the demand behaves and the way it is going to be used. The proposing energy management strategy (EMS) that we are proposing will control the total power flow of the crane. Therefore, understanding and modeling the RTG crane's typical power demand is quite important.

The complete power system of a conventional RTG crane is shown in Figure 2.1. This chapter is only focusing with the power consumers. The goal is to build a model of a typical power consumption of a conventional crane during operation.

2.1. Power Consuming Sub-systems

RTG cranes use electric motors to power its mechanical subsystems. Unlike the situation of a hybrid vehicle, its combustion engine is used to generate electricity for sub-systems. The crane has several major power consumers which makes comparatively different demand profile compared to hybrid vehicle. The power demand due to combination of following sub-systems which are displayed in Figure 2.1.
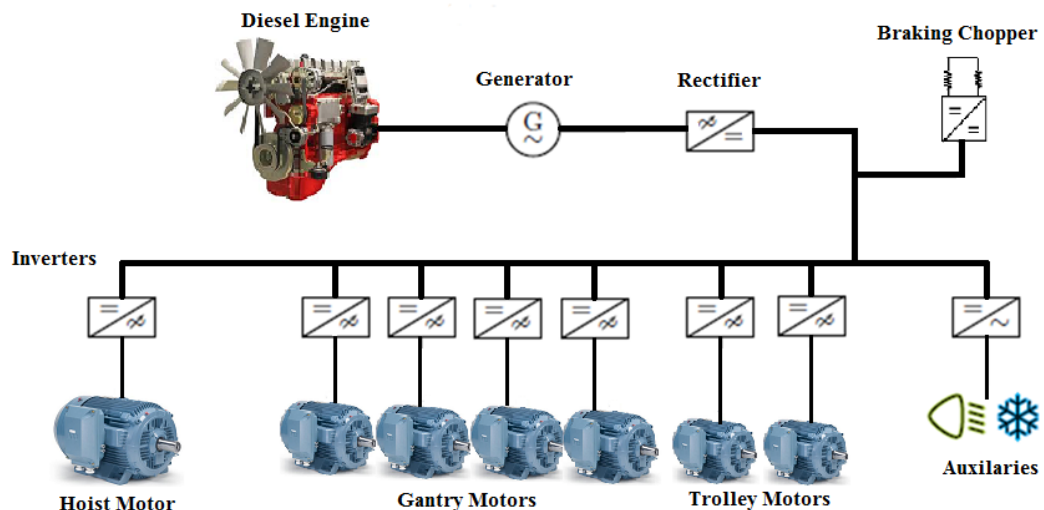
Figure 2.1 : Power system of a conventional RTG crane

- The hoist mechanism is powered by a single induction motor rated between 160-220kW, which is capable of overloading 1.8pu.

- The gantry system is driven by 4 induction motors. These motors are heavy duty motors capable of 25kW each.

- The spreader and control cabin suspend beneath the trolley where control cabin have full visibility of the spreader. Two rails are mounted on main girders to support trolley wheels. There are several trolley power configurations, such as front axle driving mechanism a with single motor, two motors independently driving front two wheels and two independent motors to drive front axle and rear axle.

- Air-conditioning systems, lights for night time operation, control power and wheel turning hydraulic pump motors contribute to auxiliary power requirements. Depending on environment variables such as outdoor temperature and daylight, these systems have constant power demand of 10-30kW.

During operation of the crane, all subsystems contribute to the total power demand. The hoist, gantry and trolley motors only need power when they are moving while the auxiliary systems are always on. The modeling of sub-systems are discussed in next section.

2.2. Hoist System Modeling

The hoist sub-system is the major power consumer within a RTG crane. Typically, RTGs have maximum speed of 50-55 m/min during hoisting and lowering under no load where maximum hoisting and lowering speed is reduced as weight of the container increases [4], [5].

Several hoist roping mechanisms are used by different manufacturers during designing RTG cranes. For example, 8 rope non- parallel mechanism and parallel rope arrangement are shown in Figure 2.3 and Figure 2.2. In MATLAB modeling, parallel rope arrangement is considered due to its simplicity where rope tension is not a function of lifting height. Due to the changing angle of ropes of non-parallel mechanism, hoisting power becomes a function of lifting height and rope tension. A mathematical discussion on 8 rope non-parallel arrangement is presented in [6].

The hoist system consists of a hoist gear-box, service brake system, hoist motor, head-block, spreader, rope drum, and a hoist inverter. Most of the designers and builders use a single induction motor as the hoist power train which is rated between

170kW and 200kW. Speed and torque requirements are matched by coupling the hoist motor to a step-down gear-box having a ratio of 1:122.9 [5]. The service brake system and electric motor is connected to high speed shaft of the gearbox the rope drum is connected to the low speed shaft. Almost all components are mounted on the trolley except the motor inverter.

Figure 2.2 : Parallel rope arrangement
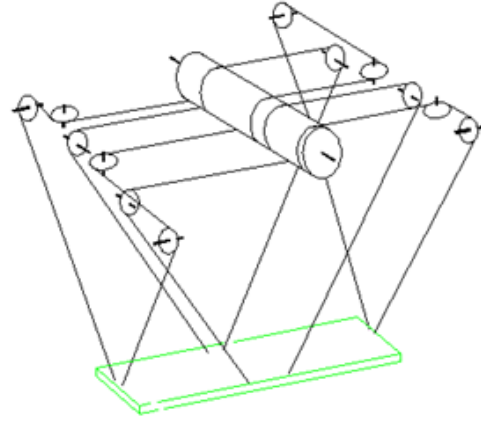
Figure 2.3 : Non-parallel arrangement

Hoisting machinery have constant power characteristics while hauling loads against gravity. Therefore, during system design and integration process, field-oriented control technique is used for hoist motor controlling due to its satisfactory performance in dynamic response. The total force excreted by the hoist drivetrain (F_h) is expressed as,

$$F_h = F_r + m_{sc}g + m_{sc}\frac{dV_h}{dt} \tag{1}$$

where F_r is the friction between the rope and hoist drum, m_{sc} is the container and spreader mass, g is the gravitational acceleration and V_h is the container velocity. The power requirement for the hoist operation (P_h) and the hoist drum angular velocity (ω_d) can be derived as,

$$\omega_d = \frac{V_h}{r_d} \tag{2}$$

8

$$P_h = V_h.F_h + \omega_d.J_d.\frac{d\omega_d}{dt} \tag{3}$$

where r_d is the rope drum radius and J_d is the drum inertia. Hence, the hoist system output power (P_1) and torque (τ_1) can be derived as follows.

$$P_1 = \omega_{hm}.J_{hm}.\frac{d\omega_{hm}}{dt} + \frac{P_h}{\eta_{GB}} \tag{4}$$

$$\tau_1 = \frac{P_1}{\omega_{hm}} \tag{5}$$

where ω_{hm} and J_{hm} are the hoist machine motor angular velocity, inertia respectively and η_{GB} is the combined efficiency of gearbox and rope sleeve. The input power ($P_{in,h}$) required from the input energy sources can be calculated to determine the machine output power, considering the motor efficiency and inverter efficiency using,

$$P_{in,h} = \frac{P_1}{\eta_{motor}.\eta_{inverter}} \tag{6}$$

where η_{motor} and $\eta_{inverter}$ are efficiencies of motor and inverter respectively. The motion of hoist motor during motoring mode is described in Equations (1)-(6). During lowering, system convert potential energy to electrical energy and Equations (1), (3), (4) and (6) change follows:

$$F_h = m_{sc}g - F_r - m_{sc}\frac{dV_h}{dt} \tag{7}$$

$$P_h = V_h.F_t - \omega_d J_d.\frac{d\omega_d}{dt} \tag{8}$$

$$P_1 = P_h.\eta_{GB} - \omega_{hm}J_{hm}\frac{d\omega_{hm}}{dt} \tag{9}$$

$$P_{out,h} = \eta_{motor}.\eta_{inverter}.P_1 \tag{10}$$

where $P_{out,h}$ is regenerative power during moving a container to lower position. As shown in Figue 2.4 the hoist mechanical sub-system is integrated with a power

9

electronic system to drive the induction motor. With the help of "electric drive blocks" from the power system block set and control blocks from the Simulink library, modeling of the hoist system carried out including modeling the power network, mechanical design and its controller.

Figure 2.4 presents the hoist system developed under Simulink environment. The mechanical system consists of service brake system modeled by a double shoe brake model which operates as a service brake system that applies brake as the motor rpm reaches zero, speed reduction gear-box, shaft to rope block to model rope drum and inertia block to simulate the combined inertia of rope drum and gearbox. A fixed mass block is used to model the total mass (13000kg) of the spreader and the head-block. A variable mass block is used to model the container mass.
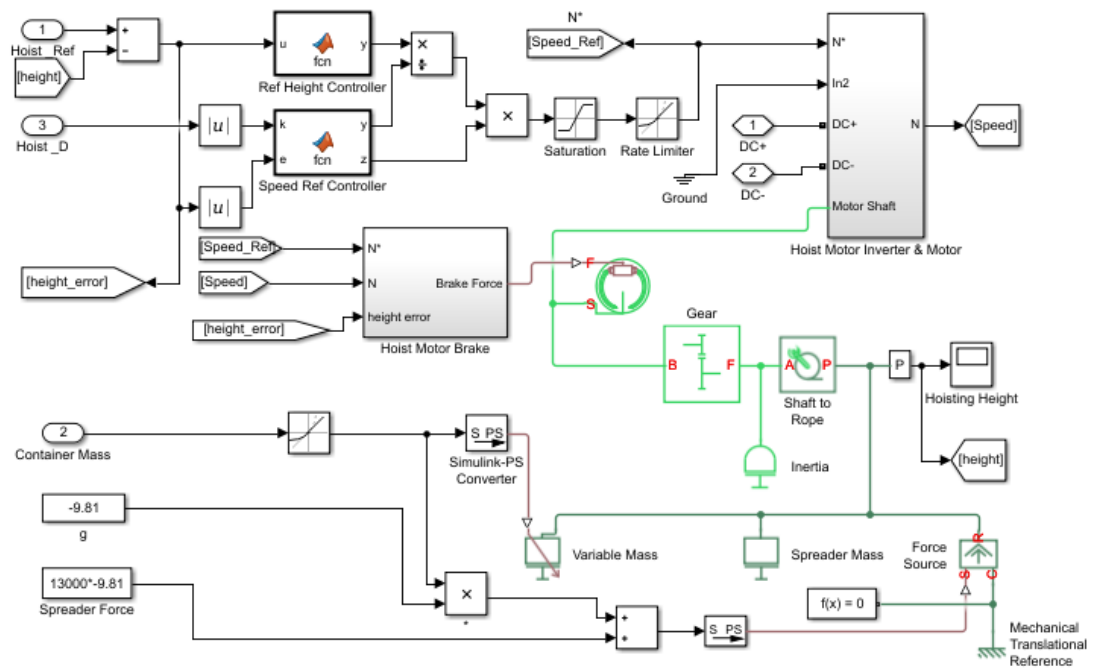
Figure 2.4 : Hoist System Model

The induction motor and inverter block shown in Figure 2.5 is the expansion view of hoist motor inverter and the motor in Figure 2.4. 180kW, 8 pole induction motor was selected as the hoist motor that operates safely below an overload factor of 1.8 when lifting a rated load.

A closed-loop field-oriented controller which is a control technique capable of providing 200% of rated torque at 0 rpm is used to model hoist motor inverter using

Electric Drive blocks of the Power System library. Use of average models to simulate the power switches (IGBTs) has increase the speed of simulation. Speed reference gradient of the speed controller was set to -375,375 rpm/s that directly controls the deceleration and acceleration of the hoist motor. Typically, RTGs are operated by human operators using joysticks which is an online event. Due to the large time lag of the simulation, the online operations by use of a control interface may not be practical in a simulation environment. Therefore, load profiles are simulated by using a programmable controller which creates hoist height reference set points according to a pre-defined operation. As Figure 2.4 displays, the hoist height reference is controlled by a closed-loop programmable controller with an inner speed loop programmable controller.
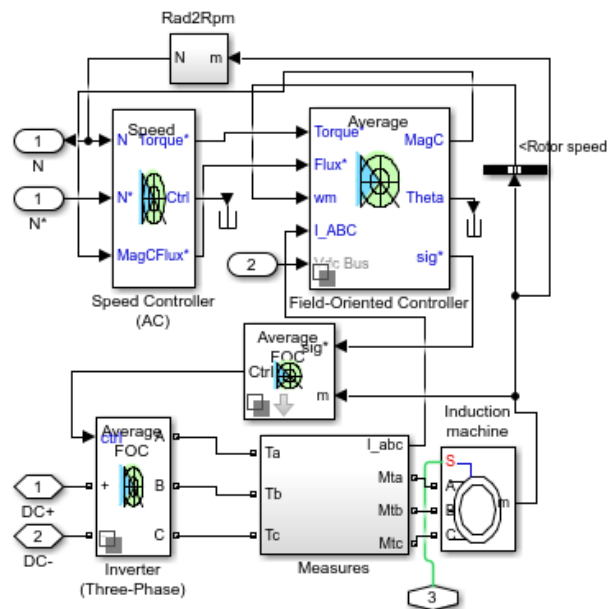
Figure 2.5 : Hoist motor and inverter

2.3. Trolley system model

The trolley sub-system consists of the head-block, control cabin and the spreader suspended beneath it. The spreader is an equipment used to attach a container using twist locks located in four corners of the spreader. The rails mounted on two main girders support as a guide way for the trolley wheels. There are three main trolley power train topologies. They are independent front axle and rear axle driving, independent front wheel driving and single motor front axle driving. The third method

shown by Figure 2.6 is modeled due to its single motor application which limit the system to a single motor drive that consequently improve the simulation speed.
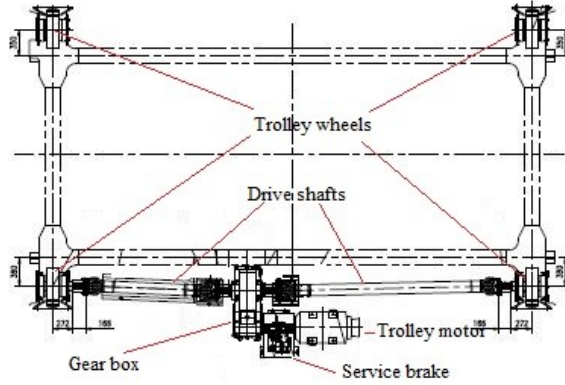
Figure 2.6 : Mechanical arrangement of trolley powertrain

The forces impose resistance the drive terrain (F_n) can be expressed as

$$F_n = F_f + F_\alpha + F_\omega \tag{11}$$

where F_f is the friction resistance due to travelling, F_α travelling slope resistance and F_ω is the wind resistance. Depending on the direction of slope and direction of wind, travelling slope resistance and wind slope resistance can act positively or negatively during operation. Therefore, simplify the modeling, the forces due to wind and slope are neglected.

$$F_n = F_f \tag{12}$$

The resultant force applying for the trolley system (F_t) is the addition of resistance force and acceleration force given by,

$$F_t = m_t \cdot \frac{dV_t}{dt} + F_n \tag{13}$$

where m_t is the total trolley mass and V_t trolley linear speed. The angular velocity of a trolley wheel (ω_w) and the motor shaft angular velocity (ω_m) can be derived

$$\omega_w = \frac{V_t}{r_w} \tag{14}$$

12

$$\omega_m = N.\omega_w \qquad (15)$$

where ω_w - angular speed of the wheels, V_t - trolley speed, N - gear box ratio and ω_m - angular speed of the motor. The power demand for trolley operation (P_t) can be derived as,

$$P_t = F_t.V_t + J_1.\omega_w.\left(\frac{d\omega_w}{dt}\right) \qquad (16)$$

where J_1 - wheel assembly inertia. The total mechanical power input (P_2) for the system is given by

$$P_2 = \omega_m.J_m.\frac{d\omega_m}{dt} + \frac{P_t}{\eta_{GB.t}} \qquad (17)$$

where $\eta_{GB,t}$ - trolley gearbox efficiency and J_m - motor inertia. The input power demanding from the energy sources ($P_{in,t}$) can be calculated to determine output power considering the inverter efficiency and motor efficiency via

$$P_{in,t} = \frac{P_2}{\eta_{motor}.\eta_{inverter}} \qquad (18)$$

Unlike the hoist mechanism, the regenerative energy content is very much limited in trolley motion. The highest recoded regenerative power in trolley system is due to deceleration. During braking equations present modeling of the system during braking where equation (19), (20), (21) and (22) express regenerative power as a positive value.

$$F_t = m_t.\left|\frac{dV_t}{dt}\right| - F_f \qquad (19)$$

$$P_t = V_t.F_t - \omega_w.J_1.\frac{d\omega_w}{dt} \qquad (20)$$

$$P_2 = P_t.\eta_{GB} - \omega_{tm}.J_{tm}.\frac{d\omega_{tm}}{dt} \qquad (21)$$

$$P_{out,t} = \eta_{motor}.\eta_{inverter}.P_2 \qquad (22)$$

13

where $P_{out,t}$ is the regenerative power during braking. Figure 2.7 shows the trolley model developed on the Simulink environment. The mechanical system consists of holding brake system modeled by double-shoe model, spool to cable to present trolley wheels and rails, sliding friction block to present dynamic friction coefficient and static friction coefficient and speed reduction gear box. A fixed mass block and a variable mass block are used to model trolley mass and container mass respectively. A 35kW, 4 pole induction motor operates through a field oriented controlled motor inverter is selected as per the manufacturer's specification.
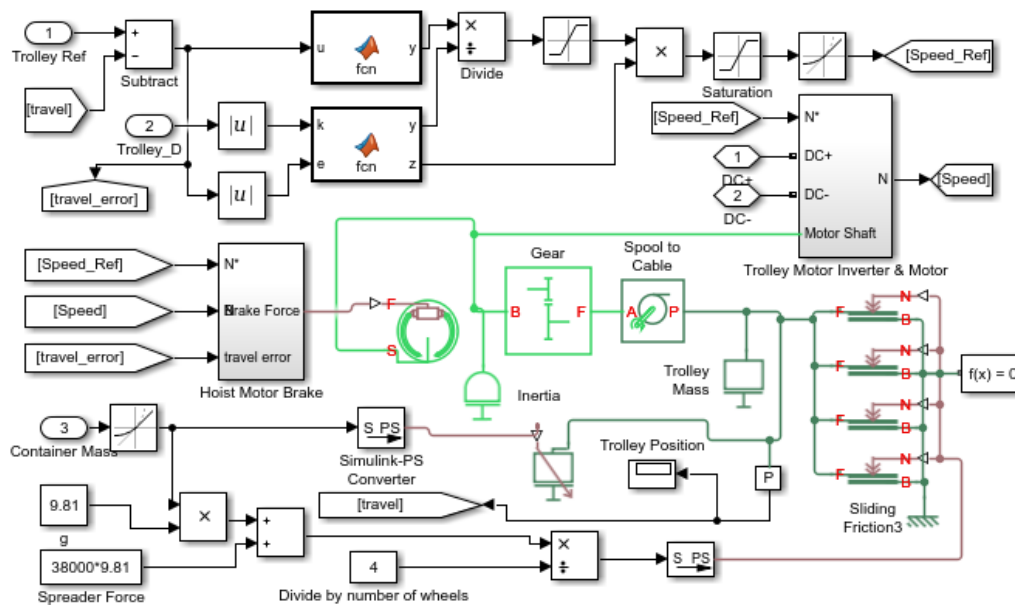
Figure 2.7 : Trolley system model

2.4. Auxiliary Power

The auxiliary systems, such as air-conditioning systems, control power, lights for night time operation and wheel turning hydraulic pump motors contribute to power requirement. These systems have more or less constant power demand of 10-35kW depending on environment variables, e.g., temperature and daylight. Considering the constant power behavior, the auxiliary power can be modeled as a constant current source depending on environment variables.

2.5. Typical Operation

The operation of a rubber tire gantry crane (RTGC) can be classified into four categories.

- Stacking a container on storage yard by unloading a truck

14

- Loading a container from the stack down to a truck
- Travelling from one row of stacked containers to another row on storage yard.
- Idling

Generally, a "move" is interpreted as a loading or unloading of a container. After a loading or unloading cycle, usually crane moves to another row for another loading cycle. In general, the contribution of the travelling function is similar to trolley function.

2.5.1. Power Demand of a Single Move

As section 2.2 and 2.3 explain, the power demand is governed by the force excreted on system, the speed of the movements and efficiency of the electromechanical system. When crane is lowering or braking the required force turns to negative where power regenerated. From 1950's various manufacturers have designed RTG cranes with different specifications to meet customer requirements. The crane used for modeling and simulation is a standard size crane which has following specifications as shown in Table 2.1.

Table 2.1 : Crane Specifications

Parameter	Configuration/Setting
Gantry span	6 wide + truck lane
Lifting heights	1 over 6
Lifting capacity	40t
Hoist speed	26m/min with rated load
Hoist acceleration	2s, rated load
Hoist deceleration	2s, rated load
Trolley travel speed	70m/min
Trolley acceleration and	4s
Gantry travel speed	90m/min
Gantry acceleration deceleration	4s

Figure 2.8 shows the modeled power demand during a loading cycle. When the power demand is positive, the crane must supply power to the electric motors. During the

sections where the power demand is negative, energy is released to the power system. In conventional RTGCs this excess energy is dissipated in a dynamic braking resistor.
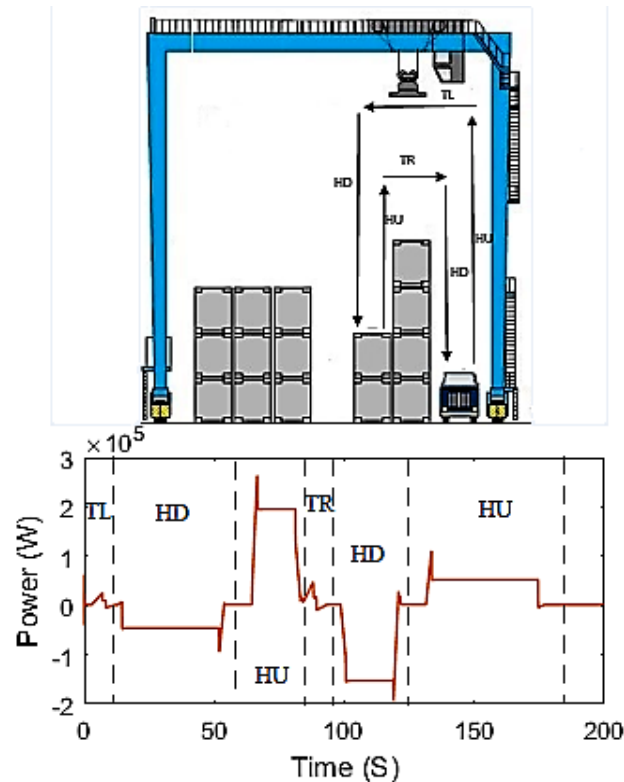
Figure 2.8 : Power demand during loading activity (TL: trolley left, HD: hoist down, HU: hoist up, TR: trolley right)

Besides the steady state power demand during each move, the motors need to accelerate to overcome inertia of rotating parts such as cable drum and brake disk. This creates a peak extra power demand at the start of each movement.

2.5.2. Quiet and Busy Operating Conditions

During operation the number of container moves per hour is solely determined by the level of activities mainly depends on the number of ships on dock, whether ships are mainliners or feeder vessels, number of containers waiting to handle, weather condition, available equipment (number of cranes under maintenance) scheduled time window of docked ships.

Typically, when mainliner ships are docked, containers are loaded and unloaded as quickly as possible creating a busy activity level inside container terminal.

Arrival of feeder vessels or empty dock create relatively quiet operating condition where cranes spend a lot of idling time between moves. Generally, this idling period varies from 150s to 250s limiting 10-12 moves/hour. Even though the power demand is only 10-30kW, during longer idling time, the diesel generator (DG) is kept on supplying auxiliary systems.
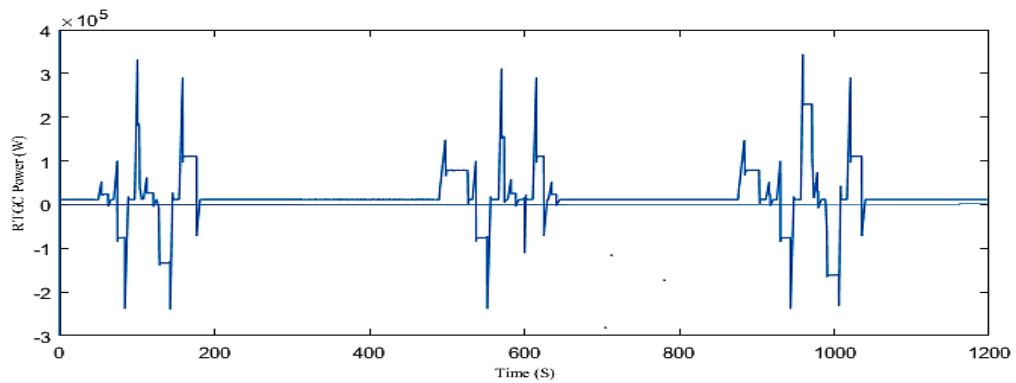
Figure 2.9 : Quite operation power profile

The demand model presented is not capable of producing 100% accurate power demand for each specific movement. The goal of the modeling is to use it as a simulation of the power demand of the crane while it is loading and unloading different containers so the energy management strategy (EMS) have realistic input signals to work with. For the purpose of following two demand models are accurate enough to validate the proposed energy management strategy. The power profiles have been simulated for 1200s which corresponds to complete operation of driving cycle.
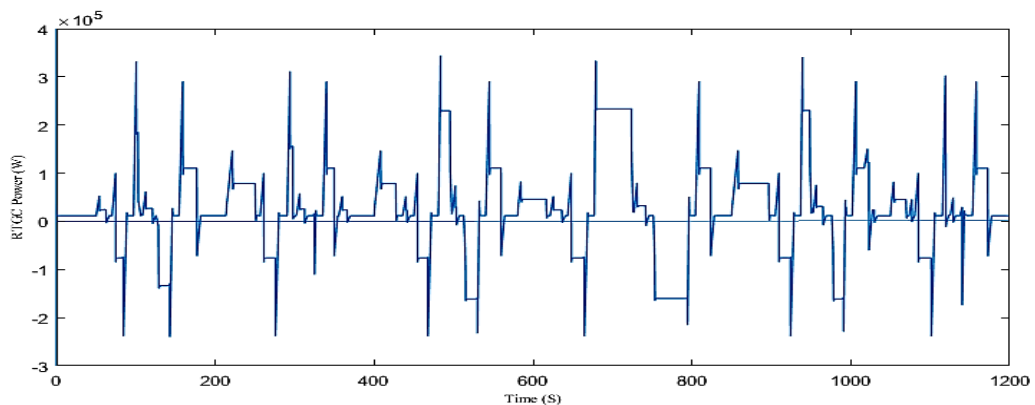
Figure 2.10 : Busy operation power profile

17

Figure 2.9 relates to quite operating condition where only three moves are handled within 20min period. During that period 30kW of auxiliary power is considered to simulate the worst-case scenario. A busy operating condition is shown in Figure 2.10 where 6 moves are done within 20min period. The most energy consuming move is also included within the system combined with 30kW auxiliary demand.

3. HYBRID POWER SUPPLY MODEL

The section two starts stepping towards the simulator for the hybrid crane by creating the demand model. The architecture of the crane was discussed in general. The upcoming step for the research is to create a model for the power supply. The power supply system has three sources on board namely diesel generator, SC bank and Li-ion battery bank. This chapter is split in a similar way as previous section. Section 3.1 discuss the model goals and move to Sections 3.2,3.3 and 3.4 to discuss modeling and sizing of Li-ion battery bank, SC bank and diesel generator respectively.

3.1. Model Goals

The proposed power system consists 3 energy sources as shown in Figure 3.1. the main power consumers are the electric motors and the auxiliary system like air conditioning, lighting and control power. The power demand of these systems was discussed in previous chapters. These three power sources of the proposed power system having their own energy reservoir where the diesel generator has its fuel tank, Li-ion battery bank has chemically stored energy and supercapacitor bank has electrical charge stored in the capacitors. The battery bank and supercapacitor bank have ability to store regenerated energy during lowering and braking.

The goal of the energy management strategy (EMS) to reduce the fuel consumption and increase the life time of the storage system. This is done by controlling the set points for diesel generator, supercapacitor bank and battery bank. Therefore, the model developed in this section is derived to the crane, developing relations between current set points for DG, SC bank and battery bank.

3.2. Variable speed DG-battery-SC hybrid System

The proposed topology for the hybrid RTGC powered by VSDG, battery and SCs is shown in Figure 3. All these energy sources are integrated through DC/DC converters, which connect them to the capacitive DC bus. Furthermore, system includes a dynamic braking resistor to dissipate excess power.

The VSDG is the primary energy source of proposed hybrid system. The generator output is connected to unidirectional active rectifier which raises the 3ph AC voltage to standard DC bus voltage. Contrarily, a rechargeable Li-ion battery bank and an SC bank are used as energy storage system.
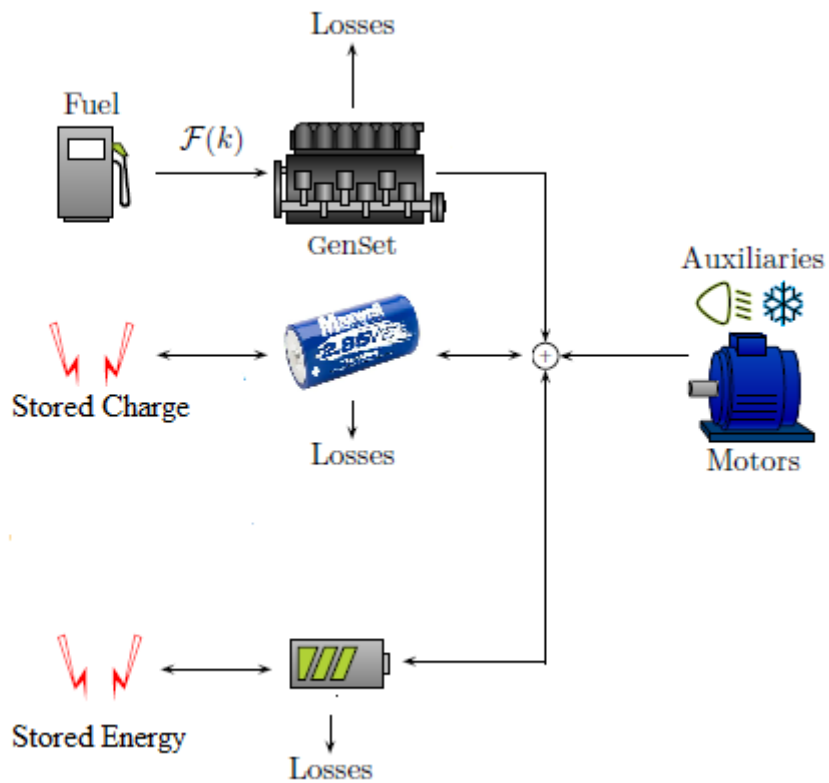
Figure 3.1 : Overview of proposed hybrid system
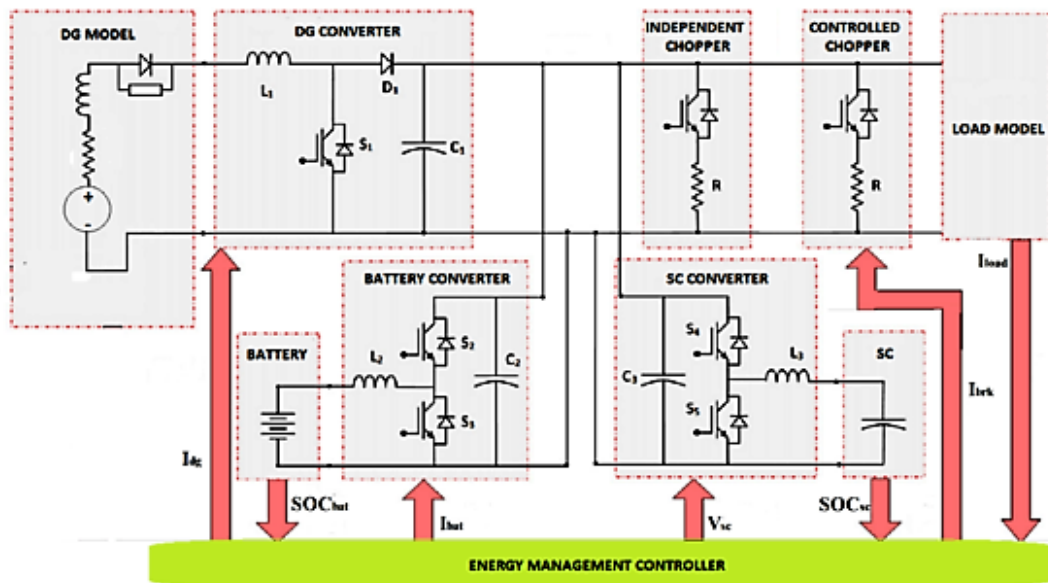
Figure 3.2 : Configuration of proposed hybrid RTGC model

The battery is used to supply extra power when needed and to supply power during idling period. A considerable amount of energy can also be recovered during lowering and braking. Because of the high dynamic response of the SC bank, it can inject or absorb peak power notches that cannot be supplied from battery and VSDG.

3.2.1. Battery Model

Batteries are heavily utilized as energy storage device in many applications. Presently hybrid vehicles, hybrid ferries, hybrid equipment (cranes), shunters and tramways are equipped with various types of batteries such as Li-ion, Ni-Mh, Ni-Cd and Pb-Acid batteries. Li-ion batteries have better response than Pb-Acid, Ni-Mh and Ni-Cd batteries. Further-more they have higher energy density, high power density and higher life cycle. Li-ion batteries can be categorized into several sub categories according to their chemical composition. Lithium Cobalt Oxide ($LiCoO_2$), Lithium Manganese Oxide ($LiMn_2O_2$), Lithium Nickel Manganese Cobalt Oxide ($LiNiMnO_2$), Lithium Iron Phosphate ($LiFePO_4$), Lithium Nickel Cobalt Aluminum Oxide ($LiNiCoAlO_2$) and Lithium Titanite ($Li_4Ti_5O_{12}$) are some of them. GS YUASA's LIM40-7D 26.6V, 40Ah [7] battery module is considered for the hybrid RTGC battery bank. The battery module consists seven cells each having ratings of 3.8V, 40Ah. The cells are made from $LiMn_2O_4$ as the positive active material and hard carbon as negative active material [8]. The operation of Li-ion battery cell has been presented by the model in Simulink under Simpowersystems library [9]. In this model, cell is represented by its equivalent circuit, a variable source in series with a resistor. The voltage value of the variable voltage source is calculated using a discharge model and a charge model, depending on how the battery is discharged and charged. The models for Li-ion cell have been developed considering Lithium iron phosphate cell in [10] [11] [12]. The discharge model of Li-ion cell used in Simpowersystems has been developed in [13] and it can represent accurately the voltage dynamics during current variations. The cell OCV during discharging ($i^* > 0$) is given by,

$$E_{bat,dis} = E_{0,bat} - \left\{ \underbrace{K.\frac{Q}{Q - \int i_{bat}dt}.i_{bat}^*}_{polarization\ resis\tan ce} \right\} - \left\{ \underbrace{K.\frac{Q}{Q - \int i_{bat}dt}.\int i_{bat}dt}_{polarization\ voltage} \right\} + \left\{ A.\exp(-B.\int i_{bat}dt) \right\} \qquad (23)$$

where $E_{bat,dis}$ is the cell OCV (V), $E_{0,bat}$ is the battery constant voltage (V), K is the polarization constant (V/Ah) or polarization resistance (Ω), Q is the battery capacity (Ah), i_{bat} is the battery current, A is the exponential zone amplitude (V), B is the exponential zone time constant inverse ($(Ah)^{-1}$), and i_{bat}^* is the filtered current.

During charging voltage increases rapidly when cell reaches full charge. This is modeled by the polarization resistance term. Experimental results have proved that the contribution of the polarization resistance can be shifted by 10% of the capacity of the cell. The Equation (24) presents the OCV during charging of a Li-ion cell.

$$E_{bat,cha} = E_{0,bat} - \left\{ K.\frac{Q}{0.1.Q + \int i_{bat}dt}.i_{bat}^* \right\} - \left\{ K.\frac{Q}{Q - \int i_{bat}dt}.\int i_{bat}dt \right\} + \left\{ A.\exp(-B.\int i_{bat}dt) \right\} \quad (24)$$

where $E_{bat,cha}$ is the OCV during charging. Cell terminal voltage can be calculated by subtracting the voltage drop due to internal resistance from the OCV. Therefore, cell output voltage, V_{cell} can be calculated as follows:

$$V_{cell} = E_{bat} - R_{int}.i_{bat} \quad (25)$$

where E_{bat} represents OCV during discharging or charging and cell internal resistance is R_{int}. Figure 3.3 presents the actual current discharge curves for different C rates for LIM40-7D cell. The discharge curves for the model for the same C rates are presented in the Figure 3.4.
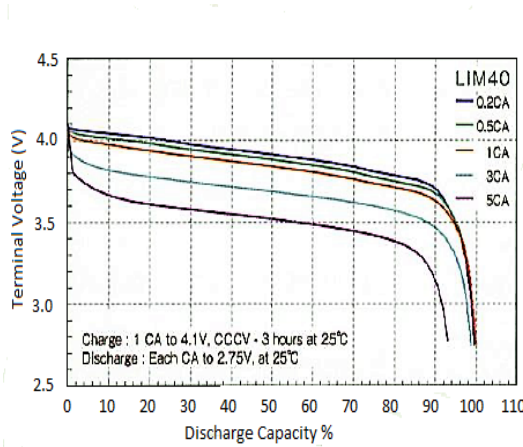
Figure 3.3 : Discharge characteristics of LIM40-7D cell [8]
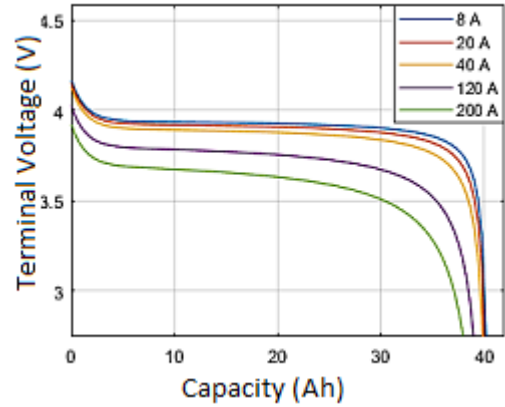
Figure 3.4 : Discharge characteristics of proposed cell model

The model characteristics do not match one to one with actual characteristics. The variations are quite large at the end of exponential zone, which may not directly influence the final design. By the way, the battery SOC must be kept between 35% and 90% to minimize capacity fade. Therefore, the energy management system will be developed to operate the system within above range, so that the battery model is considered to be valid for the design. A set of 14, LIM40-7D units is selected to

construct the battery system and all units are connected in series to obtain the maximum battery system voltage which is 372V. Battery side discharging and charging currents were limited to 150A for safe operation [7]. Referring to the above maximum discharging and charging currents, max power rating can be calculated as 55.8kW.

3.2.2. SC Model

Supercapacitors have shown their capability in energy storage for special applications. They are used in applications such as trams, trains, grid voltage stabilizers, cranes and elevators requiring rapid charge/discharge cycles rather than long term compact energy storage. Unlike conventional capacitors, SCs do not use solid di-electric, but rather they use double layer technology. The charge and discharge pulse characteristics can have current pulses as high as 1000A and their pulse duration ranges from several milliseconds to tens of seconds. SCs have pros and cons compared with Li-ion batteries. They offer high power density, high cycle life and wide operating temperature range during operation. Due to low energy density and low cell voltage of SCs, space requirements are high compared to Li-ion battery. Unlike batteries, terminal voltage of SCs varies in a broad range during operation. Therefore, a DC/DC converter should be used to interface a SC bank to DC bus. Maxwell K2 ultracapacitor cells 3.0V, 3000F [14] is considered for hybrid RTGC SC system. The cells are specially designed for heavy transport applications such as busses, cranes, rail applications etc. The operations of SC system have been presented by the model in Simulink under Simpowersystems library [15]. In this model, capacitor is represented by its equivalent circuit: a controlled voltage source in series with a resistor. The voltage of controlled voltage source is calculated using Stern equation [16] and self-discharge was neglected for simplicity. The Stern Voltage (V_t) is given by:

$$V_t = \left\{ \frac{N_s.\int i_{sc}dt.d}{N_p.N_e.\varepsilon.\varepsilon_0.A_i} \right\} + \left(\frac{2.N_e.N_s.R.T}{F} \right) \times \sinh^{-1}\left(\frac{\int i_{sc}dt}{N_p.N_e^2.A_i.\sqrt{8.R.T.\varepsilon.\varepsilon_0.c}} \right) \qquad (26)$$

where A_i is interfacial area between electrodes and electrolyte (m^3), c is molar concentration, F is Faraday constant, i_{sc} is supercapacitor current, N_e is number of layers of electrodes, N_p is number of parallel supercapacitors, N_s is number of series supercapacitors, R is ideal gas constant, T is operating temperature (K), ε is

permittivity of material and ε_0 is the permittivity of free space. Cell terminal voltage, V_{sc} can be calculated by subtracting the voltage drop due to internal resistance from the controllable voltage source. Internal resistance can be modeled as a function of temperature. In practical design, complete energy storage system includes active temperature control system. Therefore, effect from temperature fluctuations for internal resistance can be neglected. Therefore, cell terminal voltage is given by:

$$V_{sc} = V_t - i_{sc}.R_{int} \tag{27}$$

where R_{int} is internal resistance. Therefore, cell terminal voltage depends on the demand current and SC state of charge, SC_{soc} given by,

$$SOC_{sc}(\%) = \left(\frac{Q_{int} + \int i_{sc}dt}{C.V_{rated}} \right) \times 100 \tag{26}$$

where Q_{int} is the initial electric charge, C is the cell capacity and V_{rated} is the rated cell voltage.
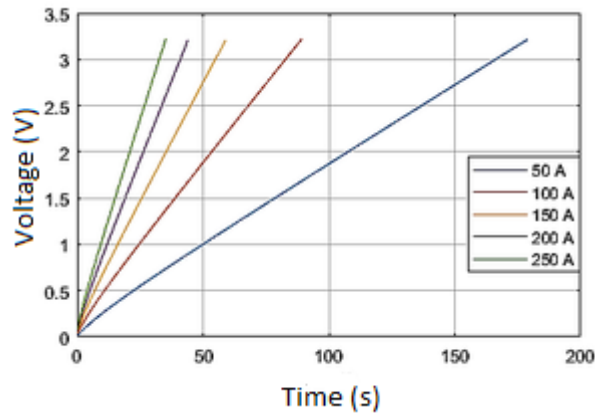
Figure 3.5 : Charging characteristics of 3.0V/3000F SC cell

Figure 3.5 shows the SC charge curves for different currents for the proposed SC model. However, the model does not exhibit any non -linear behavior as actual characteristics in [17] where tests were done for 125V, 63F Maxwell supercapacitor module. There non-linearities are quite high at low voltages compared to rated voltage in [17]. However, these non-linearities may not influence, because in practice SC systems are not drained below quarter of its rated voltage. Therefore, SC model can be considered as a valid model to represent the response of HESS.

3.2.3. Diesel Generator Model

Diesel generator (DG) is the prime energy supplier for most of the RTG cranes. Typically, a 600kVA generator [18] [19] is installed in a conventional RTGC to accommodate peak power demands. Most of the RTGCs have a DC bus to supply electrical power to all subsystems. Therefore, DG clearly operates as a DC supply rather an AC supply. Due to this configuration, dual speed generators and variable speed generators are highly popular for RTGCs where generator frequency is not a governing factor for crane system. For the proposed system a VSDG is selected. A VSDG system consist a diesel engine, synchronous generator or permanent magnet generator and a uni directional active rectifier. These systems are designed to track the most optimized fuel flow rate for a desired demand where engine speed is varied according to efficient brake specific fuel consumption. A brake specific fuel consumption equivalent to a 300kW diesel engine [20] is shown in Figure 3.6.
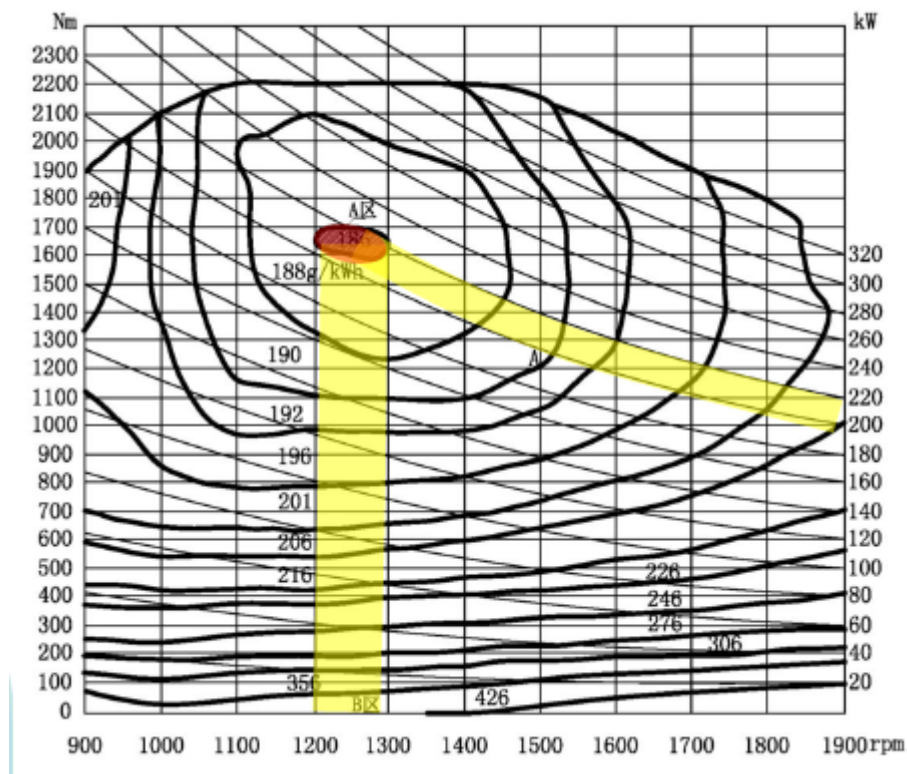
Figure 3.6 : Brake specific fuel consumption of a 300kW diesel engine

Analyzing the behavior of power demand and energy usage of diesel genset is the prime importance for the modeling. Therefore, modeling the thermodynamic behavior of the engine, dynamics of governor and controller, dynamics of the synchronous generator and AC/DC converter are ignored. DG model was created to

simulate the characteristics of VSDG with a simple unidirectional DC/DC converter which is connected to a DC source in series with an internal resistance and inductor. An operational delay and rate limiter (50A/s) were added to the model to demonstrate the power demand response. Test data for brake specific fuel consumption (BSFC) dynamics presented in [4] for a 200kW VSDG is used to estimate the fuel consumption in upcoming simulations and BSFC against power demand is shown in Figure 3.7.
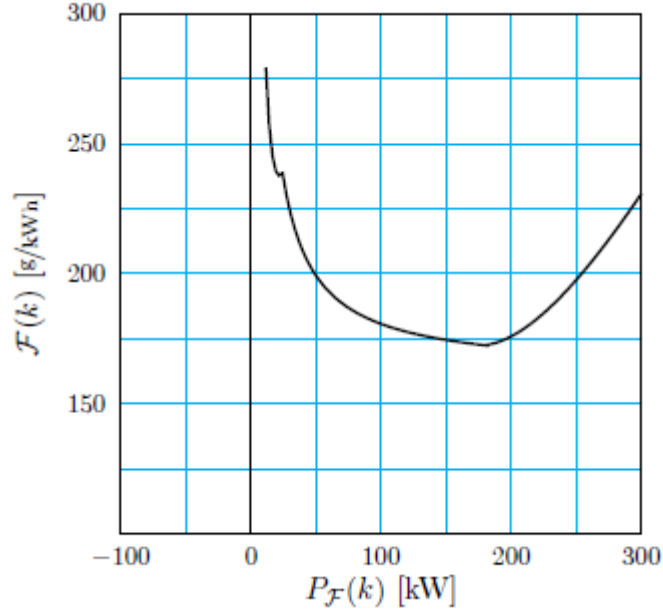
Figure 3.7 : Brake specific fuel consumption of a 200kW VSDG [4]

3.2.4. Sizing of the Li-ion Battery and its Control

Typically, batteries are popular for high energy density relative to its power density. The expected lifespan of a battery inside a hybrid system is very essential for the expected return on investment. Nowadays, Li-ion batteries are popular for hybrid application due to their high energy density and power density compared to other chemical battery technologies. There are several key factors that directly related with life span of battery cells such as ambient temperature, peak discharging currents, depth of discharge, type of DC/DC converters using to interface battery to DC-link (whether converter is a single leg drive or converter with interleaved legs), cooling system, SOC operating range and active cell balancing system.

Due to the failures on system components and violation of above mentioned limits, the effects of capacity fade can be visualized before the expected lifetime of the battery cells. During sizing of the Lithium battery system, precautions are taken to

26

minimize the effects from above factors. The maximum average power of an operation cycle is 61.6kW. Typically, this value is 24.8kW [21] due to idle time between loading and unloading cycles and due to variation of container loads. The main objective of the battery bank is to supply total crane power during idling period, absorb a portion of regenerative energy and supply 50kW continuous power (25% of VSDG capacity) to minimize the operation of the VSDG below 50kW.
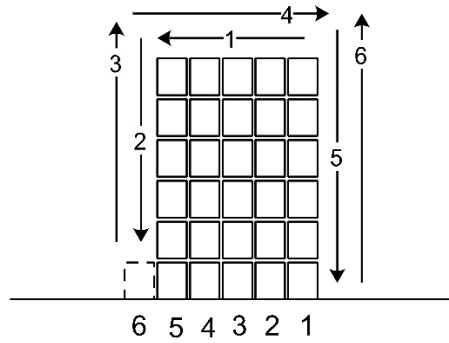
Figure 3.8 : Highest energy consuming load cycle of a RTG crane. 1. Trolley left 2. Hoist down 3. Hoist up with container 4. Trolley right 5. Hoist down with container 6. Hoist up empty spreader

GS YUASA's LIM40-7D 26.6V, 40Ah [7] battery module is considered for the battery bank. Each battery module includes seven cells with a rating of 3.8V, 40Ah. These cells are made from $LiMn_2O_4$ as the positive active material and hard carbon as negative active material [7]. These battery cells can provide 5C peak discharge current and 3C charge current at desired operating conditions. The closest battery bank voltage can be calculated by using equation

$$P_{bat} = V_{bat}.I_{bat} \tag{29}$$

where P_{bat} is the rated power of battery bank, V_{bat} is the rated battery bank terminal voltage and I_{bat} is the maximum allowable discharge current. If selected power capacity is 55kW and maximum charge and discharge current restrict to 3.75C, rated terminal voltage is given as 366V. A set of 14 battery modules are connected serially to construct the battery system. The constructed battery bank has a rated voltage of 372V which is closer to calculated value 366V. This battery module is connected to DC-link through 75kW bi-directional interleaved DC/DC converter restricting converter current to ± 75A on DC-link side. The battery converter operates on

controlled current mode to eliminate the battery system from high discharge and charge currents.

The energy management system controls the battery SOC level in a narrow band (40%-60%). The bottom margin of the band is kept as high as 40% to avoid 100% depth of discharge during failures. In an event of capacity fade, error tolerance of SOC estimation may be quite high which result the battery system to be deeply discharge, hence the situation is avoided using 40% SOC margin for bottom end. When the battery reaches 40% SOC, the battery is charged to the top margin using VSDG. During charging mode battery may experience 3.75C continuous current which will increase the internal temperature of the battery system. On the other hand, battery stores a part of electrical energy that is produced by the VSDG during operation. The round-trip efficiency of a battery converter system close to 85% where 15% of energy is lost during bi-directional transformation. The 20% SOC of battery bank represent approximately 2.9kWh which is higher than 20% of positive energy (3.67kWh) that is demanded by the high energy consuming operating cycle. Therefore, charging battery from VSDG to unnecessary levels may tend to increase system inefficiency is avoided by controlling battery SOC between 40% and 60%.

3.2.5. Sizing of SC Bank and its Control

Unlike batteries, supercapacitors do not use chemical reactions to store energy. These capacitors are a type of capacitors inheriting very high energy density due to its porous carbon electrodes and special double-layer dielectric materials. Current supercapacitors can have capacitance values that are thousands of times higher than conventional electrolyte capacitors. Supercapacitors can handle high peaks in power compared to batteries and flywheels which makes them most suitable source to supply transient demands. Supercapacitor systems have very low energy density compared to chemical battery systems. This make supercapacitor banks extremely expensive to equivalent battery capacities.

In proposed hybrid RTG crane, SC bank is used to supply transient power demand which is above the battery and VSDG maximum discharge current. During operations high peak currents are visible for a maximum period of 4.5s due to hoist acceleration and deceleration. There are two possible methods to respond transient demand as quick as possible. One, match the supercapacitor bank voltage and directly

connect the SC bank to DC-link where SC bank act as a low pass filter. Second, a constant voltage-controlled DC/DC convert to interface the SC bank to DC-link where DC-link voltage is maintained by SC converter. Typically, supercapacitor cell has a rated voltage between 2.7V to 3.0V and 3000F capacity. When selecting SC capacity, 5 key factors are considered.

1. *The energy content during peak transient period* (E_{peak})

    The energy required during accelerating from 0 to rated speed with rated load shown in Figure 3.9.

2. *Energy buffer* (Z)

    The energy content during peak transient period (E_{peak}) is multiplied by a factor (Z) to compensate unpredictable disturbances.

3. *Maximum energy content affected by the state transition delay* $(E_{t-delay})$

    State control machines introduce time delays between two state transitions to avoid toggling between states. During some state transitions delays (t_{delay}), SC bank must supply the demand to avoid power swing on demand.

4. *SC (state of charge) SOC bottom margin* $(SOC_{lower-m\arg in})$

    SC SOC is tightly coupled with terminal voltage. In proposed system, SC system is used to regulate DC bus voltage. DC/DC converters are most likely to drive unstable when SC terminal voltage reach bottom operating voltage margin of the DC/DC converter. Therefore, SC SOC bottom margin is selected as 30% to calculate the SC bank capacity.

5. *SC SOC operating point* $(SOC_{operating-po\text{int}})$

    SC bank primary function is to maintain DC link voltage while providing transient demand. The system also supposed to absorb regenerative transient peaks during operation. In such cases SC bank can overcharge in an event where reserved capacity is insufficient. Considering above requirements, the energy management strategy controls the SC SOC at 70%

SOC using a close loop controller where 30% of SC SOC is reserved to absorb regenerative energy peaks during lowering and deceleration.

State control machines introduce time delays between two state transitions to avoid toggling between states. To move between two states, EMS must sacrifice 200ms where SC bank should supply the energy to avoid power swing. The maximum permissible energy due to time can be calculated as follows,

$$E_{t-delay} = P_{\max} \times t_{delay} \tag{30}$$

where $P_{\max}$ is the maximum demand of RTG crane. Considering the above 4 facts, the minimum energy capacity for the SC bank can be calculated as follows,

$$SC_{capacity} = \left[\frac{\left(Z \times E_{peak}\right) + E_{t-delay}}{SOC_{operating-pont} - SOC_{bottom-m\arg in}} \right] \tag{31}$$

Thus, E_{peak} can be roughly calculated as 0.0854kWh from the enclosed area by red lines in Figure 3.9. $E_{t-delay}$ can be calculated using Equation 30 considering $P_{\max}$ as 300kW. The effective SOC range of SC bank ranges from bottom margin (30%) to its steady state operating point (70%) representing 40% of the SC bank. Although the energy losses due DC/DC converter is not directly involved with Equation 31, the buffer introduced as Z in Equation 31, is considered as 100% which compensate the unpredictable disturbances. Thus, minimum capacity of SC bank is then,

$$SC_{capacity} = \left[\frac{\left(2 \times E_{peak}\right) + E_{t-delay}}{SOC_{eff-range}} \right] = 0.468kWh \tag{32}$$
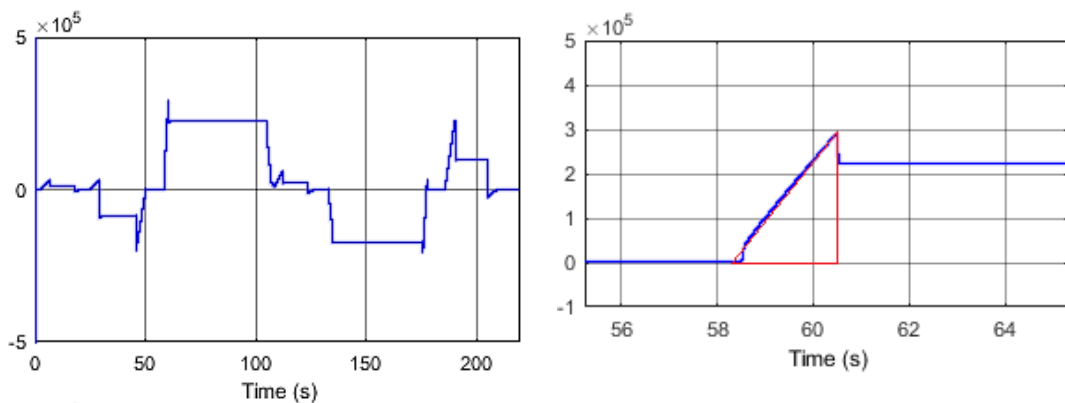
Figure 3.9 : Power ripple during acceleration of hoist system with rated load (40t)

A commercial supercapacitor developed by Maxwell is selected for the design. The cell has ratings of 3000F and 2.85V where maximum permissible voltage is 3.0V [14]. Assuming 50% energy stored inside SC cell is effective due to losses in DC/DC converter and SC cell itself due to high discharge currents (close to 500A), the number of SC cells can be calculated as follows. Considering a serially connected SC string with N cells,

$$SC_{capacity} = \frac{1}{2} \times \left(\frac{C_{rated}}{N} \right) \times \left(NV_{effective} \right)^2 \tag{33}$$

where C_{rated} is the used standard SC cell capacitance in Farads and $V_{effective}$ is cell voltage where 50% of stored energy retains inside the cell. According to Equation 33, 248 cells are required to meet the capacity. Typically, DC bus voltage of RTG cranes vary from one manufacturer to another ranging from 600VDC to 750VDC. The connection of SC cells depends on the three factors, maximum super capacitor cell voltage, number of supercapacitor cells and DC bus voltage. Considering above facts, two parallelly connected SC cells are organized to a single module and then 124 modules are serially connected to form the SC bank. Due to above configuration, maximum SC bank voltage restricted to 372V and 250kW bi-directional 3 leg DC/DC converter is used to interface the SC bank to DC-link.

3.2.6. Sizing of Variable Speed Diesel Generator and its Controls

In the matter of energy management strategy, the main purpose of the diesel generator is to supply power demand partially or fully and recharge the lithium battery under controlled conditions. Unlike conventional iso-synchronous generators, in proposed hybrid system the SC system handle transients where generator response is not very much crucial. Therefore, generator and battery bank should able to supply steady state demand of a RTG crane under 40t heavy rated container. Maximum continuous generator demand ($P_{max-gen-con}$) can be calculated as follows.

$$P_{max-gen-con} = P_{max-hoist} + P_{max-aux} - P_{bat-con} \tag{34}$$

where $P_{max-hoist}$ is the maximum steady state hoist power, $P_{max-aux}$ is the maximum auxiliary power and $P_{bat-con}$ is the continuous battery power. Thus, the peak generator continuous power is then,

$$P_{\max-gen-con} = P_{max-hoist} + P_{max-aux} - P_{bat-con}$$

$$P_{\max-gen-con} = 235kW + 30kW - 50kW = 215kW$$

<div align="right">(35)</div>

A 200kW diesel engine coupled with 250kVA alternator (standard configuration) is selected with prime power rating where 10% overload capability is available for a 1hour period within a 12-hour cycle of operation. A VSDG is a fuel-efficient solution compared to constant speed diesel generator due to the characteristics of the demand profile (generator is partially load or light loaded during most of the operating period). The common DC bus allows to interface a variable speed diesel generator (VSDG) without much effort for the system. The variable frequency and variable voltage of the generator is rectified using an active front end converter which is controlled in controlled current mode or constant voltage mode. The system adjusts the engine speed to maximize fuel economy according to real time demand.

3.2.7. DC/DC Converter Model

The terminal voltage of energy sources (SC, Li-ion battery) fluctuates according to their demanded power and SOC. Thus, a power electronic system is needed to control the output power of the sources where the power demanded by the system keeping the DC bus at constant. A special power electronic system composed of a PWM based bi-directional DC/DC converter is used to interface each energy source with the DC bus. This bi-directional DC/DC configuration allows the energy transmission in both directions, from the battery or SC to the DC bus, and vice versa. In industrial applications interleaved DC/DC converters are highly used due to their inheriting advantages on low output current ripple. During modeling, average model of a single leg DC/DC converter is used to simplify modeling. It consists of a high-frequency inductor L_2, an output smoothing capacitor C_2, and two high-frequency switches (IGBTs) S_2 and S_3, which allow bi-directional power flow as shown in Figure 3.10b. During charging mode, the S_2 switch and D_3 diode operate a unidirectional buck converter that enables power flow from DC bus to source. During discharging mode, the S_3 switch and D_2 diode operate the converter as a unidirectional boost converter that delivers power from source to DC bus.
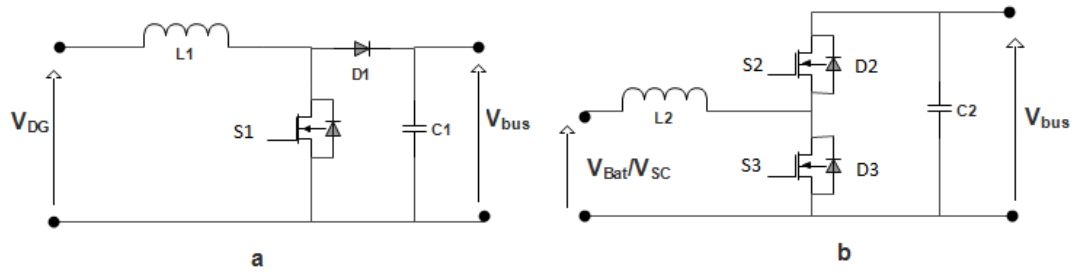
Figure 3.10 : DC/DC converters used in hybrid system: (a)Unidirectional converter (b)Bi-directional converter

A unidirectional boost DC/DC converter is used in the DG model where energy can only flow from the DG to the DC bus. This converter is operated as a controllable current source, where current set point is determined by the HESS. This converter is composed of a high-frequency inductor L_1, output filter capacitor C_1, a diode D_1 and a high-frequency switch (IGBT) S_1 as shown in Figure 3.10a. The two quadrant DC/DC converter model of SimPowerSystems [22] is used to model the converters.
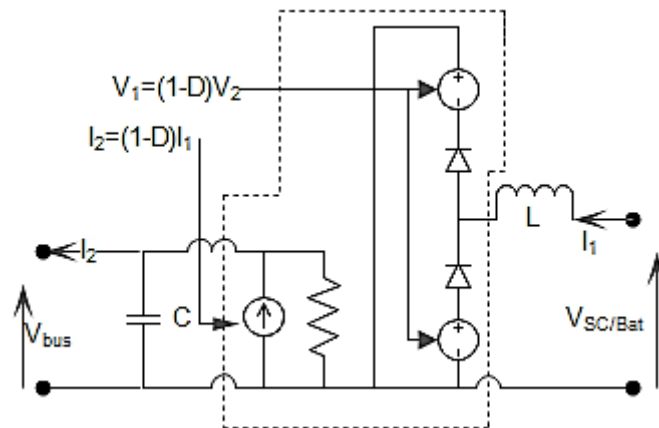
Figure 3.11 : Average-value model of DC/DC converters

Figure 3.11 shows the average value equivalent model of the converter where power electronic switches are represented by current and voltage sources. The equivalent model consists of a controlled current source at the DC bus side and a controlled voltage source at the battery, SC, or DG side. The average model provides fast simulation where switching function model is directly controlled by the duty without a PWM generator.

3.2.8. Brake Chopper Model

During lowering, most of the regenerated energy is stored in the battery and SC. However, when the battery and SC or SC itself achieve the charge limit, power absorbing capability reduces drastically. Therefore, to maintain the DC bus voltage, this excess energy must be dissipated. A braking resistor is used to dissipate excess energy where IGBT chopper is used to control the current through the braking resistor. The HESS determines the instantaneous value of power that should be dissipated within the braking resistor.

4. ENERGY MANAGEMENT STRATEGY

The former sections laid foundations for the design of energy management strategy. The intension of using such management system is clear where the modeling and sizing shows the important characteristics of the system. In this section the existing hybrid systems and their performance is discussed and second the design of new energy management system is explained.

4.1. Existing Hybrid Systems and their Performance

Hybridizing RTG cranes has been an interesting idea since early 2000 due to increasing fuel prices [23]. An important research had been conducted by USA researches adopting a 2.12MJ flywheel and a 455kW diesel generator to power a RTG crane [24]. They had used a fly wheel which is comprised of high speed permanent magnet synchronous machine and its motor drive to recover and re-use regenerated energy in crane applications. Experimental data had revealed that a 20.9% reduction in fuel consumption had been achieved. An important contribution from Korean researches who adapt a 4.19MJ supercapacitor bank and 120kW diesel generator is described in [25]. They have used 3 interleaved 250kW bi-directional DC/DC converter to interface SC bank to DC-link. Due to the small capacity of DG, it runs mostly in an efficient area compared to highly rated DGs used in conventional RTG cranes. The small capacity of the DG has not affect the stability of DG, because SC bank operate in constant voltage mode which react transients. The researches had achieved 35% reduction in fuel consumption by experimental validation.

Another important work is the contribution of Netherland researches who adopt hybrid energy source comprising of a variable speed diesel generator (VSDG) and 1.38 kWh custom made supercapacitor bank is discussed in [4]. The variable speed diesel generator rated at 300kW comprise a smart controller who adjusts engine speed according to demand. Under light loading constant speed diesel generators have high brake specific fuel consumption which make them extremely fuel inefficient in light load and idle condition. The smart controller in VSDG lower the engine speed in light load and idle condition which reduce the fuel consumption drastically. The power share from VSDG is calculated using equivalent consumption minimization strategy (ECMS) and engine start stop strategy also has been adopted. By adopting ECMS+

feedback strategy for controlling the hybrid system, researches have achieved 52.2% fuel reduction in operation.

A commercial hybrid system (sybrid system) developed by Japanese researches comprised of a hybrid energy source equipped with small capacity constant speed diesel generator and a small capacity lithium battery bank to power a RTG crane [3]. The diesel generator has a power rating of 130kW where auxiliary systems directly connected to DG. The battery bank is developed by series connection of twenty GS YUASA LIM30H Li-ion battery modules having rated terminal voltage of 576V with 30Ah capacity. These battery modules are specially designed for high power applications such as locomotives, electric buses automated guided vehicles and cranes where they can be charged and discharged at 20C (600A). Therefore, battery can be considered as a 345kW power source at its maximum performance. A bi-directional charge discharge controller is placed between battery bank and DC-link to control the operation of battery bank. Due to the direct connection of auxiliary power to DG and small capacity of battery bank, diesel generator runs mostly in an efficient area compared to conventional RTGs. With the solution, an average 50-60% fuel reduction is achieved.

Another commercial hybrid system developed by Norwegian engineers adopt a hybrid energy source equipped with small diesel generator rated at 50kW with 91kWh battery bank [26]. During the idling period diesel generator is forced to shut down and allows RTG to operate on full electric mode. The system has proven 65-75% reduction in fuel consumption in operation.

4.2. Energy Management System (EMS)

The existing hybrid systems are designed using constant speed generators combined with either supercapacitor/battery systems or variable speed diesel generators combined with either SC/battery bank. Due to the inherent characteristics of SCs and batteries, sizing high energy capacity with SC system or sizing high power battery system may not be an economically viable solution. Most of the existing hybrid systems consist SC bank with very low energy capacity where crane have to de-rate its performance when SC bank reach its critical level. Systems with batteries have low life span due to high pulse current discharges which are beyond its recommended conditions. Reaching very low SOC levels or overcharge conditions during faulty

conditions or abnormal conditions can reduce the available capacity (capacity fade effect). The proposed system uses SC sub-system to filter transient demand from VSDG and battery system while energy management system using a unique technique to keep battery system under healthy condition. Typically, battery systems are constructed connecting individual cells in series or parallel to match the voltage and capacity. When maintaining terminal voltage of a large serially connected battery bank, cell voltages may differ due to various facts. To avoid large deviations in cell voltages, cell balancing systems are adopted. Due to the imperfections of these systems, control algorithms or abnormalities on some cells, still there is a high chance that some cells experience overvoltage when battery bank SOC reach close to 95% which accelerate capacity fade effect of the overvoltage cells. During lower SOC levels some cells reach low cell voltages due to SOC estimation errors or malfunction in balancing system. Unlike pure electric vehicles, hybrid systems have flexibility to select and modify battery SOC operating region. Operating battery bank SOC under a narrow band can reduce the potential of risk reaching over voltage and under voltage condition for individual cells even under faulty conditions and abnormal conditions. Table 4.1 presents the capacities of individual components and their control limits.

Table 4.1 : Hybrid System Specifications

Parameter	VSDG	SC	Battery
Rated Current (A)	300	100	40
Max Current (A)	330	500	150
Current slew rate (A/s)	50	-	100
SOC (min)	-	70%	40%
SOC (max)	-	25%	60%
Control mode (CCM, CVM)	CCM	CVM	CCM
Capacity	350kVA	48.3F	40Ah
Rated voltage (V)	600	334	372
DC bus voltage (V)		680	

This section has been organized in four subsections. The top three sub-sections describe the operation of VSDG, SC and battery. The last sub-section explains the state machine controller which generate the appropriate reference control signals for VSDG, battery, SC and braking chopper processing the input states of SC state of charge, battery state of charge and real time demand current which is sampled at a rate of 10kHz.

4.2.1. VSDG Control

VSDG has poor time response compared to constant speed generators. Typically, VSDG maintains engine speed closer to idle speed during no load condition. According to real-time, demand the system adjusts the engine speed optimizing fuel consumption as shown in Figure 4.1. In practice, discrete speed set points are given for optimal power ranges [27] and even under light load conditions VSDG maintains considerable high fuel efficiency [28] compared to constant speed generators. VSDG converter, (active AC/DC rectifier in actual system) can be controlled in two modes, namely controlled current mode and constant voltage mode. The modeled system operates as a controlled current source where dynamic current variation restricted to 50A/s. The slow dynamic response (50A/s) helps to reduce partially burned exhaust gas during engine loading and modeling can be simplified to equivalent DC source with series internal resistance and inductance. The fuel consumption test data published in [4] is used to model the fuel consumption dynamics along with total consumption for proposed simulations. The maximum current is set to 330A in which generator is overloaded by 10%. A PI controller regulates the current output according to the setpoint given by the EMS.
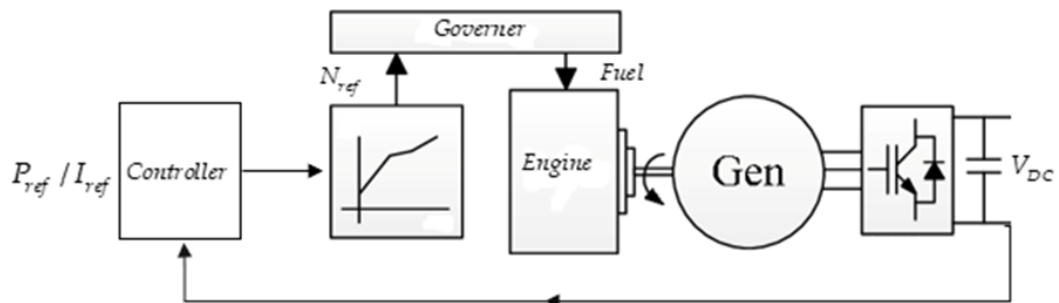
Figure 4.1 : VSDG Architecture

4.2.2. SC Control

The SC converter operates as a constant voltage controller which primarily maintains the DC bus voltage. A close loop PID controller determines the suitable duty factor for the SC converter to maintain the DC bus voltage, where SC bank voltage varies heavily with SOC level. As the system demands power from the SC bank while trying to maintain the DC bus voltage, the duty cycle of the SC converter increases so that the SC bank voltage decreases, and the SC bank is discharged.
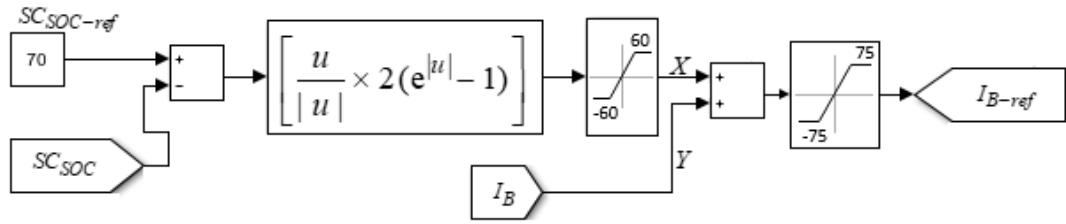
Figure 4.2 : SC Charge Controller

Two types of peaks are possible within the system during operation, positive power peaks due to acceleration and negative power peaks due to deceleration. The negative power peaks do not contain much energy. Trying to save energy of negative power peaks during deceleration may not be economical. But during acceleration, energy for positive power peaks must be supplied to avoid degrading performance of the system. To cope with uncertainty of power peaks, SOC of the SC should be maintained at a higher value. During the design process, a SOC level of 70% is selected considering negative transient regenerative energy impulse during hoist deceleration and positive transient energy impulse (0.0854kWh) due to hoist acceleration. The SOC level of the SC bank is maintained by controlling the power flow of the battery bank via proposed numerical estimator shown in Figure 4.2 where I_{B-ref} represents the control command for battery converter. Therefore I_{B-ref} is given by,

$$I_{B-ref} = \left[\frac{u}{|u|} \times 2\left(e^{|u|} - 1\right)\right] + I_B \tag{35}$$

where u is the SOC error and I_B, battery current command from state controller. The numerical estimator generates a bounded (± 60) exponential current reference according to SC SOC error. During operation, the demand current determines net current that SC bank may charge and in some instant a considerable time lag may be introduced during continuous high demand currents.

4.2.3. Battery Control

The battery control determines the suitable duty cycle of the battery converter to maintain the current requested by the EMS, while the battery terminal voltage varies depending on the operating mode (charge or discharge) of the battery. The battery side current is limited to 150A (3.75C) for discharging and charging. The battery current

reference (I_{B-ref}) is coupled with two parameters, namely SC SOC level and demand current as discussed in Figure 4.2 and Equation 35. The priority is given to demand current where remaining current portion is naturally absorbed or give out by the SC DC/DC converter due to its constant voltage control mode.

Usually industrial LI-ion battery systems are managed by battery management systems (BMS). BMS individually monitor each cell voltage and balance if necessary. Typically, BMS systems are responsible for estimating state of charge of the battery systems. In proposed system, battery SOC is controlled by the state machine controller and a SOC level-based hysteresis band is introduced as the charging and discharging algorithm. Three different charge discharge scenarios are introduced by the state controller as shown below.

1. Charge the battery bank from VSDG up to 60% (upper margin) SOC, when bottom margin detected by the state controller
2. Support the steady state demand along with VSDG until SOC reach its bottom margin (40%)
3. Interrupt the charging process and contribute to demand when demand current extensively high. (e.g. When demand current reach above 270A)

The battery SOC level is controlled in a narrow band 40-60% to avoid 100% deep discharge during failures. During the operating lifecycle a tolerable capacity fade could introduce SOC estimations errors which may lead battery system to be deeply discharge. Hence the situation is avoided using 40% SOC margin for the bottom end. During charging mode, battery bank experiences a 3.75C continuous charging current that may increase the internal temperature of the battery system. 60% upper SOC margin limit the charging capacity approximately to 2.9kWh (>1.86kWh, average electricity consumption per move for electrified RTGC) which controls the heat generated during constant current charging while minimizing the energy losses due to round trip efficiency of the battery and converter system.
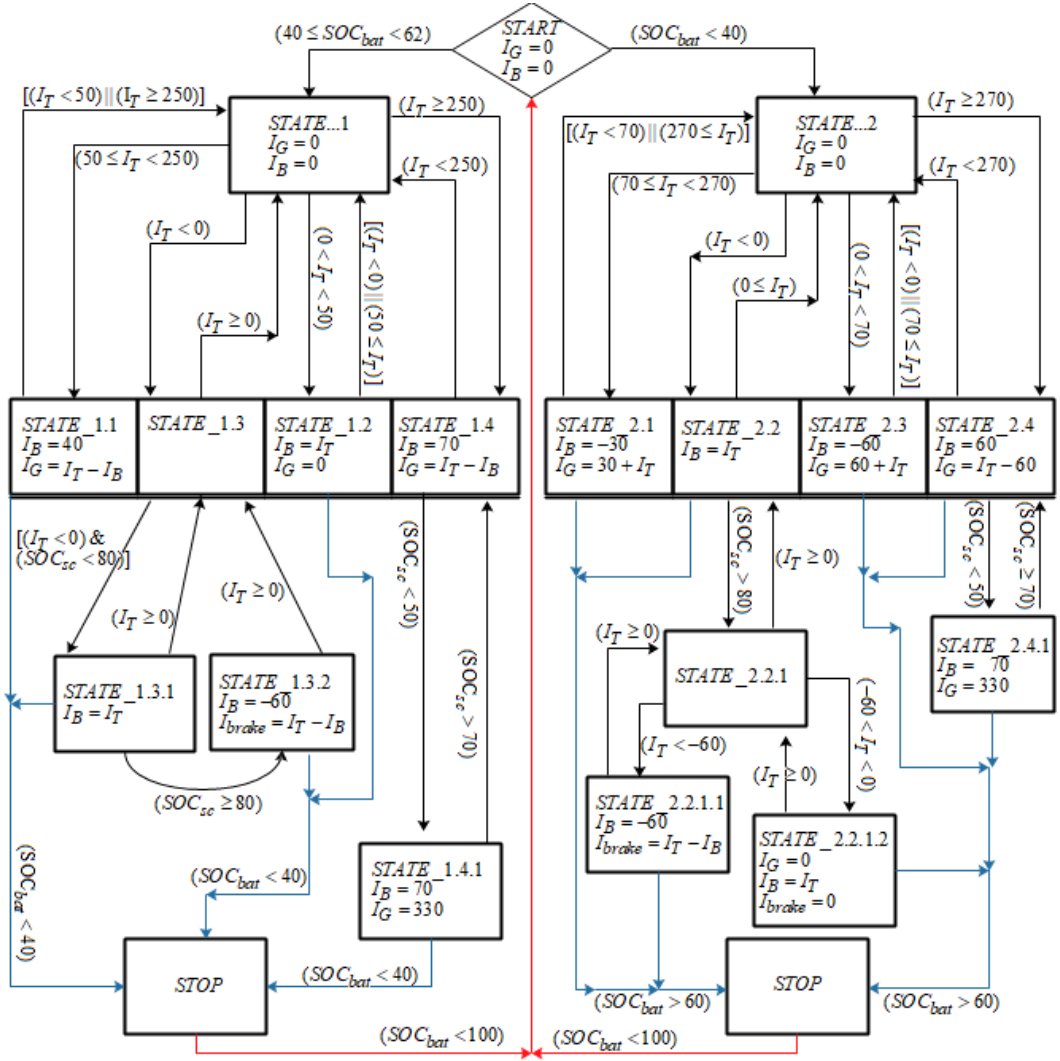
4.2.4. State Machine Controller

In Figure 4.3 the decision-making process of the state machine is displayed. The state machine control has the advantage that it is relatively easy to understand what is happening in the process of selecting the set points for Li-battery, SC and VSDG. State controller is mainly based on two states to decide the operating point for each converter

of the hybrid system. Two levels of battery SOC have been considered: low SOC (<40%, state 2) and normal SOC (40%-60%, state 1) where battery SOC is controlled within a narrow band of 20%. The algorithm generates reference current set points for VSDG, battery and corresponding current command for power to be dissipated in the dynamic braking resistor. Since the VSDG dynamic response is low, the system tries to avoid the rapid changes in the VSDG system. The changes in the reference current set points will occur when system components reach their limits. The controller determines the operational state according to the demanded load of RTGC sub systems and battery SOC level. Battery SOC is maintained between 40% and 60% while SOC of SC is maintained at 70%.

The structure of state controller is shown in Figure 4.3 where I_G is generator current set point, I_T is total current feedback from the system, I_B is battery current set point, I_{brake} is current set point for braking chopper, SOC_{bat} is the SOC of battery and SOC_{sc} is the SOC of SC. A time delay is introduced between state transitions to avoid toggling between states. During time delay, the additional power requirement is supplied by the SC bank. the operation of two main conditions are described as below. The time delay was set to 0.2s to minimize the effects on state of charge of SC. The operation of two main states is described below. The total steady state current demand of the system is given by,

$$I_T = I_G + I_B \tag{36}$$

where, SC current is not considered due to its absence in steady state. Therefore, supercapacitor current is not present with the diagram and all operational states shown in state diagram full-fill the requirement of Equation 36 here onwards.

Figure 4.3 : State Machine Controller

State 1(left side of the diagram):

When SOC_{bat} is between 40% and 60% VSDG operates as an adaptive source. During above battery SOC level,

$$I_T = I_B \tag{37}$$

where total current demand (I_T) is less than 50A (state_1.2). As the total demand increases above 50A, VSDG operates as an adaptive source except for one condition where $(I_T \geq 250 \ \& \ SOC_{sc} \leq 50\%)$ shown by state_1.4. The battery and VSDG current set points can be given as (state_1.1 and state_1.4),

42

$$I_G = I_T - I_B; (50 < I_T \le 250) \tag{38}$$
$$I_B = 40$$

$$I_G = I_T - I_B; (250 < I_T) \tag{39}$$
$$I_B = 70$$

The battery converter current reference (I_{B-ref}) is given by,

$$I_{B-ref} = I_B + I_{sc-soc-charge} \tag{40}$$

where $I_{soc-sc-charge}$ is the charging current reference output by the SC charge controller defined as X in Figure 4.2. The state_1.4.1 refers to sub-condition where SC_{soc} drops below 50% during $(I_T > 250)$ and VSDG is forced to deliver its maximum power (330A) until SC_{soc} reach 70%. During energy regeneration SC operates parallelly with battery where there is no limitation for regenerative power level given by,

$$P_{re-gen} = P_{bat-charge} + P_{sc-charge} \tag{41}$$

where P_{re-gen} is regenerative power, $P_{bat-charge}$ is charging power of battery and $P_{sc-charge}$ is charging power of SC. State_1.3.1 equalize the total demand current to battery current where battery converter limits it to $\pm 75\,A$ where rest of the current naturally absorbed by the SC system due its constant voltage operation. When SC reaches its max energy level (80%), the extra regenerative energy is dissipated in the braking resistor as shown in Equation 42 and state_1.3.2,

$$I_B = -60$$
$$I_{brake} = I_T - I_B \tag{42}$$

where I_T is negative during regeneration.

State 2 (right side of the state diagram):

When SOC_{bat} drops below 40%, VSDG charges the battery system up-to 60% except energy regeneration mode and situations where demand current (I_T) exceed 270A as

shown in state_2.4.1. During low demand $(I_T \leq 70)$ the VSDG current reference and battery current reference is given by,

$$
\begin{aligned}
I_G &= -60 + I_T; (I_T \leq 70) \\
I_B &= -60
\end{aligned}
$$
(43)

where battery is charged from VSDG at an approximate rate of 40kW which is almost 20% of VSDG rating. The VSDG and battery current references during $70 < I_T \leq 270$ can be given as

$$
\begin{aligned}
I_G &= 30 + I_T; (70 < I_T \leq 270) \\
I_B &= -30
\end{aligned}
$$
(44)

When the demand current exceeds 270A margin, battery supports the system as shown in state_2.4 and progressing to state_2.4.1 depending the SC SOC condition. During energy regeneration the system operating logic shown in state_2.2, state_2.2.1, state_2.2.1.1 and state_2.2.1.2 is similar scenario discussed in Equation 42, operating parallelly SC and battery to absorb energy and dissipate energy in braking resistor when SC reaches its max SOC level.

5. SIMULATION RESULTS

The proposed hybrid system and the control strategy have been implemented in MATLAB-Simulink and tested for power profiles shown in Figure 2.9 and Figure 2.10. The system has been simulated for 1200s which corresponds to complete operation of driving cycle. Figure 2.9 relates to quite operation condition where only three moves are handled within 20min period. During that period 30kW of auxiliary power is considered to simulate the worst- case scenario. A busy operating condition is shown in Figure 2.10 where 6 moves are done within 20min period. The most energy consuming move is also included within the system combined with 30kW auxiliary power demand. To evaluate the EMS under different operating conditions, four simulations were performed covering full range of battery SOC with different demand profiles. The first two simulations demonstrate the system behavior when battery SOC reach bottom margin and third, fourth simulations cover the behavior when the system starts operating mid SOC range.

A) Simulation with an initial battery SOC of 38% with quiet operation.

B) Simulation with an initial battery SOC of 38% with busy operation.

C) Simulation with an initial battery SOC of 50% with quiet operation.

D) Simulation with an initial battery SOC of 50% with busy operation.

The proposed VSDG capacity and its operation mode plays a major role to minimize the fuel consumption. The fuel consumption during 4 cases are evaluated using test data published in [4]. The 4 simulation cases record 3.66L, 4.36L, 3.38L and 4.06L fuel consumptions respectively. An event combining all 4 cases as a single event can be considered to have a broader view about fuel consumption. The event presents a total of 18 moves within 80-minute period where total consumption calculated as 15.4L. The fuel consumption per move is recorded as 0.85L/move. The above result is calculated with 40 hybrid RTG cranes that include 200kW VSDG and 13.8kW battery bank [27]. The batch of cranes had recorded a consumption of 1.175L/move averaging consumption of 2,218,729 moves in 2016. The simulation results present a 27% reduction compared to hybrid system discussed above and 57.5% reduction compared to conventional RTG crane where conventional cranes consume 2L/move.

5.1. Case 1: Simulation with an Initial Battery SOC of 38% with Quiet Operation

In this case, it was considered an initial battery SOC of 38%, so that the battery starts to charge to upper SOC threshold, in which both the charge and discharge of the battery and SCs are allowed. Quiet load profile was simulated on the system where Figure 5.1 shows the SOC variations of battery and SC, the current variations of DC bus, battery, SC and VSDG. A distinct variation between SOCs of battery and SC can be seen where battery SOC has a smooth profile due to its higher energy capacity. SC SOC variations have a broader band due to its low energy capacity. Maintaining SC SOC is important because charging above 100% could destroy the SC and discharging below 25% could make unstable the DC bus voltage. In Case 1, SC SOC is maintained between 95% and 25% where DC bus voltage is unaffected. The fast-dynamic response of SC makes the battery and VSDG currents smooth where battery discharging and charging currents limits (-75A/75A) are maintained as expected. The VSDG's 50A/s slew rate needs 6s to reach rated power. However, this slow response has not affected to the system operation during Case 1 while maintaining the limits as expected.

5.2. Case 2: Simulation with an Initial Battery SOC of 38% with Busy Operation

In this case, the battery starts to work with low SOC of 38%, and therefore, its discharging current must be minimum as Case 1. The simulation results are shown in Figure 5.2. During the first 350s, the battery gets charged due to its low initial SOC and therefore, EMS adapts sub-states of state 2 where battery is forced to charge by the VSDG. From 350s to 750s the battery supports the system by discharging and charging during regeneration. During regeneration, EMS moves to state_1.3.1 and state_1.3.2 to charge battery and SC and dissipates excess energy through the braking resistor. SC and battery have similar behavior to Case 1 without violating the defined constraints. According to Equation (37), Equation (38) and Equation (39) the EMS changes its response to meet the demand.

5.3. Case 3: Simulation with an Initial Battery SOC of 50% with Quite Operation

This case was simulated with an initial battery SOC of 50%, so that battery starts to work with a normal SOC, in which both the charging and discharging of the battery are allowed. Figure 5.3 shows the SOC variations and current variations of energy sources. During 20min period, two discharge and charge cycles can be seen from the battery SOC graph. Battery current variations were low compared to Case 2, due to higher idling period as in Case 1. System operates as expected within defined boundaries.

### 5.4. Case 4: Simulation with an Initial Battery SOC of 50% with Busy Operation

This case was simulated with an initial battery SOC of 50% with busy power profile. At initial point of start, battery discharging, and charging are allowed. Figure 5.4 shows the SOC variations and current variations. Maximum peak demand of VSDG, 330A had been recorded during the operating period of the highest energy demanding move. Large SOC variations of SC can be seen similar to Case 2, which had taken much longer time to recover. During the simulation period, all important parameters such as SC SOC, DC bus voltage, battery current and VSDG current had not violated their designed rules.
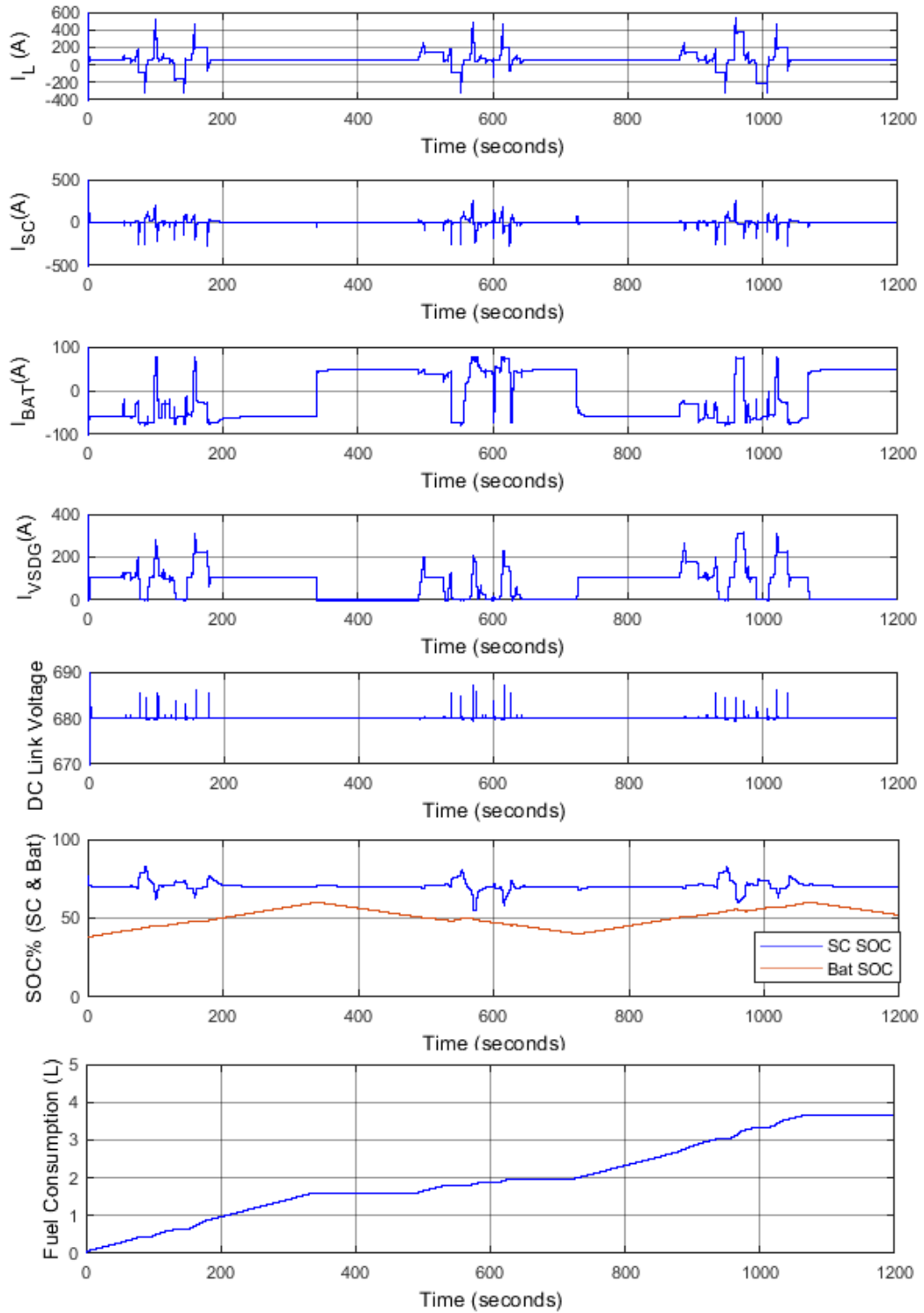
Figure 5.1 : SOC and current variations of Case 1
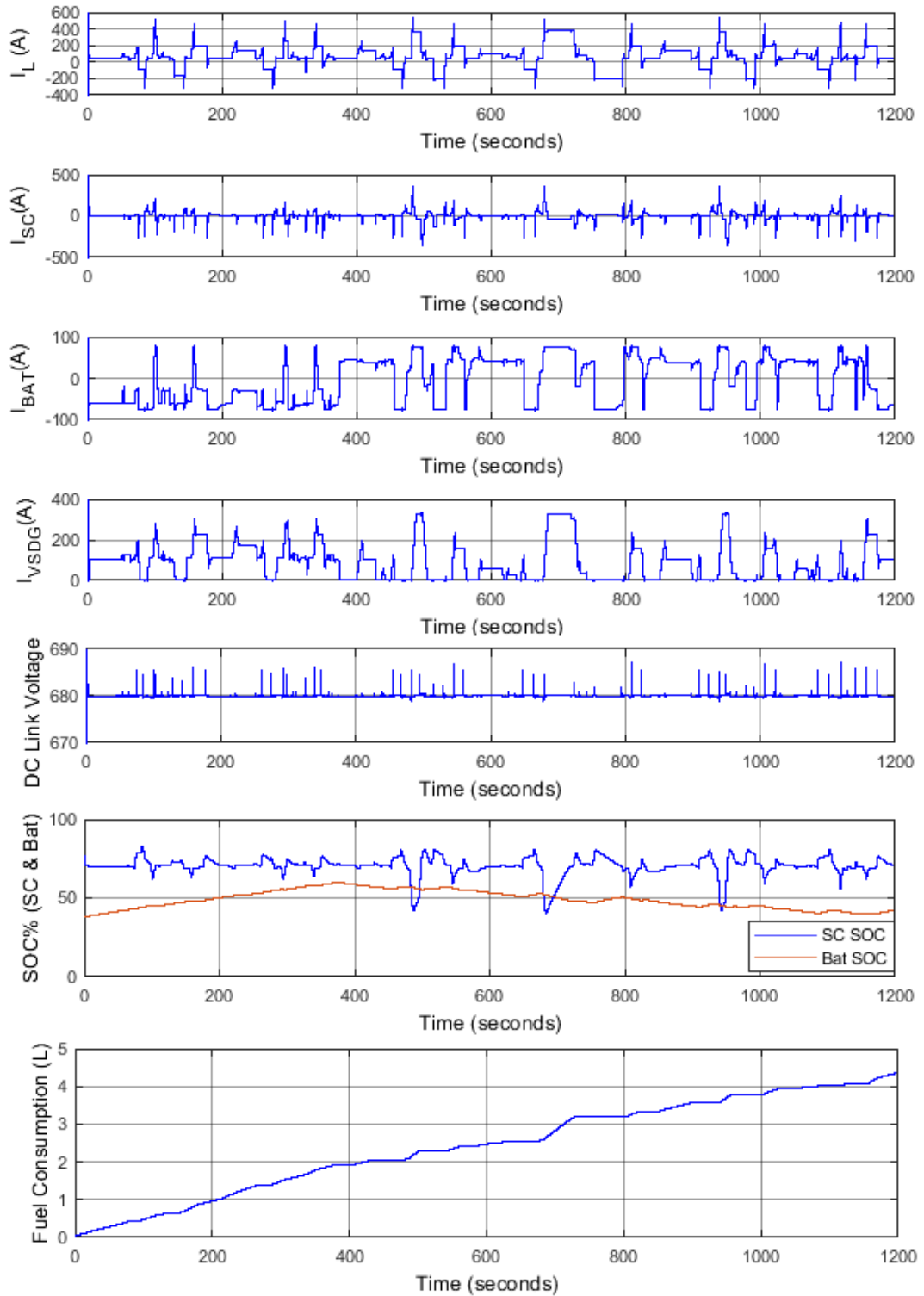
Figure 5.2 : SOC and current variations of Case 2
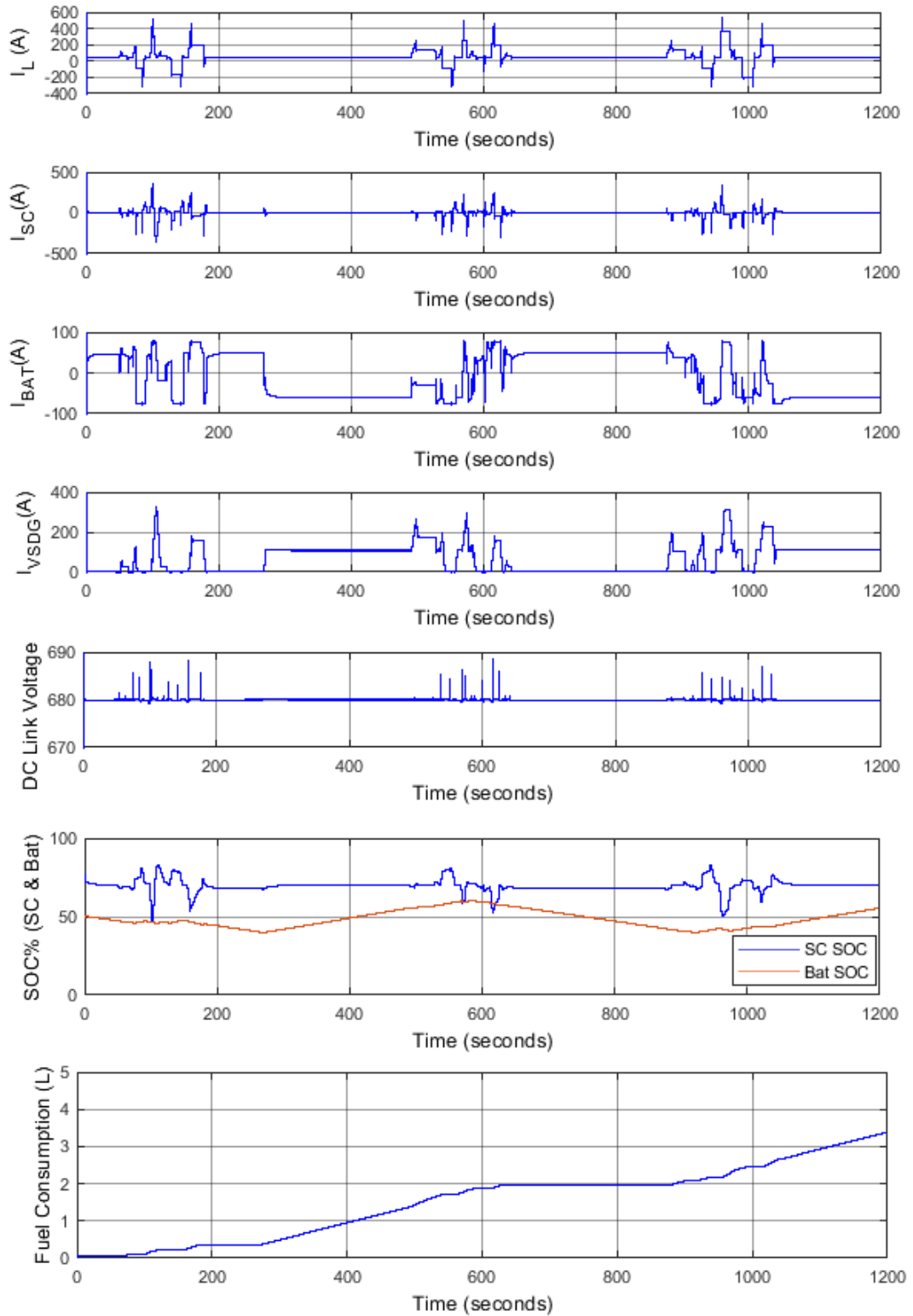
Figure 5.3 : SOC and current variations of Case 3

Figure 5.4 : SOC and current variations of Case 4

5.5. Discussion

The proposed configuration for the hybrid system and the EMS safely operates with a 200kW VSDG which is downsized by 50% compared to conventional generator capacity. The simultaneous operation of VSDG, SCs and battery have potential to supply total demand including 500A current peaks. Lower generator capacity and its variabl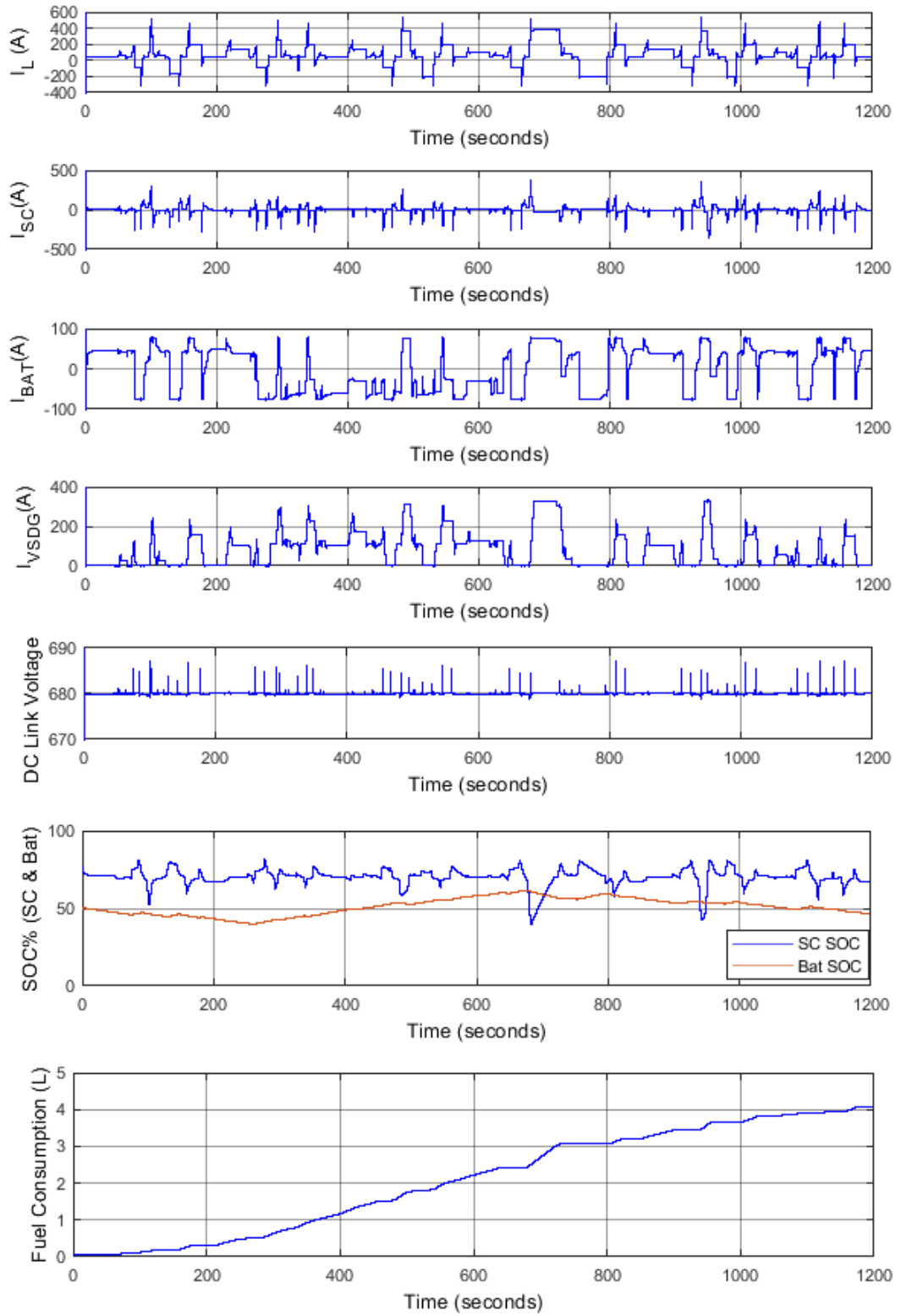e speed operation are the main dominant factors for fuel saving. Instead of using conventional constant speed 400kW generator, proposed system uses 200kW variable speed genset. During simulations, 50A/s rate of increase was introduced to simulate the low dynamic response of VSDG. Throughout the time of operation on 4 Cases, system did not progress to any unstable conditions. High SC SOC distortions can be seen in Case 2 and Case 4 where average power requirement is at its highest value. Lower SOC valleys of SC had taken considerable time to recover due to high power demand (above 350A) by the container move. The VSDG loading, fuel consumption and fuel consumption per move are presented on Table 5.1.

Table 5.1 : Diesel Consumption and generator loading

Case	Fuel Consumption (L)	Fuel Consumption per move (L/move)	Battery SOC transition cycles	VSDG loaded time (s) (active time)	VSDG loading more than		
					50kW (s)	100kW (s)	150kW (s)
Case 1	3.66	1.22	3	719.5	666.1	114.3	55.6
Case 2	4.3	0.71	2	772.8	602.2	247.7	130.1
Case 3	3.38	1.13	3	674.7	607	120.4	37.6
Case 4	4.06	0.67	2	716.7	573.7	231.3	107.6

The battery SOC transition cycles represent the complete transitions that Li-ion battery had undergone either charging from 40% to 60% or discharging 60% to 40%. The Case 1 and Case 3 have recorded 3 transitions in quiet operating condition due to pure electric mode operation to supply auxiliary power during crane idle period. A considerable deviation between fuel consumption per move can be seen in quite (Case 1 and Case 3) and busy (Case 2 and Case 4) conditions due to low generator loading above 150kW margin which can be clearly visible on "VSDG loading more than

150kW" column in Table 5.1. During all 4 operating cases, VSDG had maintained a load above 50kW for more than 75% of its active time.

The results demonstrate that the proposed hybrid system and EMS allow the RTGC to properly follow the driving cycle. In this paper, we have obtained good results for the RTGC following its operating cycle. Using three power sources namely VSDG, SC bank and battery connected to DC bus via AC/DC and DC/DC converters enable the EMS to actively control the power flow and achieve stable system which can operate continuously.

6. CONCLUSIONS AND RECOMMENDATIONS

In the beginning of this section conclusions for previous chapters are presented. Section 6.2 discuss the possibilities for further research in the contest of energy management systems for RTG cranes.

6.1. Conclusions

Electrical system suppliers for port equipment are facing tough competition to keep innovating and deliver superior products. In container handling business, hybrid applications and electrified applications are steadily growing keep up with terminal automation, strict environmental regulations and to reduce operational costs incur due to consumption of petroleum-based fuels in large volumes. This thesis focusses on improving operational lifetime of battery-based hybrid RTG systems by restructuring the hybrid architecture with additional super capacitor bank and proposing a new energy management strategy. The main subject is formulated as follows.

How can an energy management system and hybrid storage system will enhance the lifetime of the energy storage system and maintain the fuel efficiency that is promised by the existing hybrid RTG crane systems?

To answer the above question, it was split to three objectives covering the broad area starting from section of energy storage devices for hybrid storage system to development of energy management strategy and validation of system performance through simulations.

6.2. Simulator

6.2.1. Power demand simulator

The mathematical model of RTG crane with its power demand was analyzed in Section 2. All crane motions are powered by a set of 3ph induction motors where hoist motor is the powerfullest of all. The peak power demand of the crane predominantly dominated by the hoist acceleration and acceleration time which creates power peaks up to 292kW and large amount of regenerative power during lowering. The power peaks can be differentiated considering the difference in the duration of these peaks for loading and unloading from yard tractors, due to the height difference between the tractor-trailer and stack. Typically unloading a container from yard tractor generally

requires more net energy than loading where container is moved down considering higher distance.

In between container moves, the crane can be idle depending on the busyness. During those idling periods, the auxiliary system still demands 15-30kW of power. The long idle times can have a large impact or minor impact depending whether crane is conventional, supercapacitor-based hybrid or battery-based hybrid.

6.2.2. Power supply model

Power supply model of RTGC is discussed in Section 3. The model consists three parts, a variable speed diesel generator, Li-ion battery bank and supercapacitor bank. The modeling complexity of each sub-system is considered according to dynamic behavior and power control topologies used to control the output power.

VSDG is modeled as DC source with an internal resistance and inductance connected to unidirectional DC/DC converter. A slow rising and falling rate (50A/s) is introduced to avoid large step changes which could lag the diesel engine where fuel consumption may be too complex to reproduce in simulations. Steady loading and de-loading also keep the internal fuel combustion process which eventually increase the fuel efficiency. The consumption of VSDG is calculated by mapping the power demand with brake specific fuel consumption test data presented in [4].

The Li-ion battery bank can store and deliver power in steady state. A model was created based on Matlab/Simulink and tuned to data provided by the manufacturer. The battery bank connected to the DC-link through a bi-directional DC/DC converter to the DC bus.

The supercapacitor bank can store and deliver small amount of energy with high power ratings for short durations. The SC model was created, based on data from manufacturer and Sc model presented in Simulink/Model. The efficiency of SC system depends on the current flowing through it. Therefore, a fully charged supercapacitor bank is much more efficient than when it is nearly empty. A bi-directional DC/DC converter is used to interface the Sc bank to the DC-link.

6.2.3. Energy Management System

The proposed energy management system is discussed in Section 4. The control algorithm is based on state machine control technique which have advantages against

other techniques. Achieving optimum fuel efficiency does not always produce most economical system. The operational and maintenance costs both highly influence the economical behavior throughout the operating period. State machine control systems are difficult to tune for optimal performance. But these systems can be easily implemented, modified and troubleshoot logic errors, easily. The EMS generate current control reference points for VSDG converter, battery converter and controlled braking chopper evaluating battery state of charge, SC state of charge and demand current. The system has three operating modes embodied inside the controller. The system operates in full electric mode when battery SOC is higher than bottom margin and demand less than 50A. Hybrid mode operation when demand exceed 50A current and battery SOC higher than bottom margin. Charging mode operation when battery SOC reach bottom margin of the battery bank. The SC bank DC/DC converter configured to operate on CVM where VSDG, battery and braking chopper converters operate on CCM. Current slew rates are introduced to VSDG and battery converter to slowdown the response during step load changes. During such occasions (accelerations and decelerations), the demand is naturally supplied by the SC bank.

The EMS limits the battery SOC operating range to 20% which is beneficial in few ways. The round-trip efficiency of charging Li-ion battery from VSDG and supplying power from battery is comparatively low although it very important for hybrid operation. On the other hand, Li-ion batteries have capacity fade effect when they are subjected to deep discharge and overcharge conditions. Although, battery management system is used to overcome this issue, measurement errors, hardware faults and parameter changes in RTGC can deeply discharge or overcharge the Li-ion battery bank. The selection of 40% to 60% SOC can minimize the effects and increase the workable life time of the battery system.

6.2.4. Simulation Results

The simulation results are discussed in Section 5. Four simulation cases were selected covering whole spectrum to validate the system operation. In all 4 simulation cases highest possible auxiliary demand was selected to simulate the worst-case scenario. During all 4 simulation cases the proposed system behaved as expected without moving to unstable regions (DC bus under-voltage due low SC bank SOC). The results of various parameters are presented in Table 5.1 including fuel consumption. The VSDG has operated above 50kW (25% of VSDG capacity) load

margin more than 75% of its loaded time where light loading time has been considerably reduced. The simulation results presented in Section 5 also revealed that the proposed system can be more efficient compared to hybrid system discussed in [27].

6.3. Recommendations

The presented work focused on researching and improving lifetime of battery-based hybrid RTG cranes. The results are inspiring, but there are substantial things left for future research. A true scale hardware system-based test should be performed to accurately measure the system performance. The model of the power system that was developed in this thesis is far good enough for simulation, but still it is not perfect. There are many energy management topologies which can be embodied with narrow SOC operating range. Therefore, further improvements with new strategies might also be possible.

REFERENCES

[1] Statista, "Container Shipping - Statistics & Facts, Colombo," [Online]. Available: https://www.statista.com/topics/1367/container-shipping/.. [Accessed 13 November 2018].

[2] Hybrid Vehicle Drivetrain, "Series hybrid," [Online]. Available: https://en.wikipedia.org/wiki/Hybrid_vehicle_drivetrain.. [Accessed 13 November 2018].

[3] M. H. S. Sumithomo Heavy Industries, "SYBRID System, Hybrid Technology for Rubber Tire Gantry Cranes," [Online]. Available: http://www.shi.co.jp/shi-mh/english/technical/sybrid.html. [Accessed 13 November 2018].

[4] H. Hellendoorn, S. Mulder and B. D. Schutter, "Hybrid Control of Container Cranes," in *Proceedings of the 18th IFAC World Congress*, Milan, Italy, 2011.

[5] "Calculation Book for Rubber Tyred Gantry Container Cranes for CICT," Shanghai Zhenhua Heavy Industry Co. Ltd, June 2013.

[6] S. Pietrosanti, W. Holderbaum and V. M. Becerra, "Modeling Power flow in a Hoist Motor of a Rubber Tyred Gantry Crane," *Industry Applications Society Annual Meeting,* vol. 52, pp. 2088-2094, 2016.

[7] S. koen and M. ku, "Lithium ion battery for industrial use," GS YUASA International Ltd., Tokyo, Japan.

[8] T. Inoue, K. Nishiyama and W. A. Moll, "Large-sized Li-ion Battery Module for Hybrid Powered Energy System," 24 April 2007. [Online]. Available: http://citeseerx.ist.psu.edu/viewdoc/download?doi=10.1.1.390.154&rep=rep1&type=pdf.

[9] "Simpowersystem Blocks, battery," Matlab, 2018. [Online]. Available: https://in.mathworks.com/help/physmod/sps/powersys/ref/battery.html?searchHighlight=Battery&s_tid=doc_srchtitle. [Accessed 6 October 2018].

[10] N. Omar, M. A. Monem, Y. Firouz, J. Salminen, J. Smekens, O. Hegazy, H. Gaulous, G. Mulder, P. V. d. Bossche, T. Coosemans and J. V. Mierlo, "Lithium iron phosphate-based battery – Assessment of aging parameters and development of cycle life model," *Applied Energy,* vol. 113, pp. 1575-1585, 2004.

[11] L. Saw, K. Somasundaram, Y. Ye and A. A. O. Tay, "Electro-thermal analysis of Lithium Iron Phosphate battery for electric vehicles," *Journal of Power Sources,* vol. 249, pp. 231-238.

[12] C. Zhu, X. Li, L. Song and L. ". Xiang, "Development of a theoretically based thermal model for Lithium ion battery pack," *Journal of Power Sources,* vol. 223, pp. 155-164.

[13] O. O. Tremblay and L. Dessaint, "Experimental validation of a Battery Dynamic Model for EV applications," *World Electric Vehicle Journal,* vol. 3, 2009.

[14] *Datasheet K2 Ultracapacitors – 3.0V/3000F,* San Diego, USA: Maxwell Technologies Inc.

[15] "Simpowersystem Blocks, supercapacitor," Matlab, 2018. [Online]. Available: https://in.mathworks.com/help/physmod/sps/powersys/ref/supercapacitor.html. [Accessed 22 August 2018].

[16] K. B. Oldham, "A Gouy-Chapman Stern model of the double layer at a (metal)/(ionic liquid) interface," *Journal of Electroanalytical Chemistry,* vol. 613, pp. 131-138, November 2007.

[17]   P. Gracia, J. P. Torreglosa, L. M. Fernandez and F. Jurado, "Viability study of a FC-battery-SC tramway controlled by equivalent consumption minimization strategy," *International Journal of Hydrogen Energy,* vol. 37, pp. 9368-9382, April 2012.

[18]   "One Rubber-tired gantry container crane for port Hambantota-Mechanical calculation," Shanghai Zhenhua Heavy Industry Co., Ltd, May 2014.

[19]   "Rubber-Tired Gantry Crane for Sri Lanka Project-Mechanical Calculation," Shanghai Zhenhua Heavy Industry Co., Ltd, June 2008.

[20]   "Explore Exchanges for Further Upgrade Transformation Technical solutions of CICT E-RTG," CMinnotech, February 2017.

[21]   W. Niu, X. Huang, F. Yuan, N. Schofield, L. Xu, J. Chu and W. Gu, "Sizing of Energy System of a Hybrid Lithium Battery RTG Crane," *IEEE Transactions on Power Electronics,* vol. 32, no. 10, pp. 7837-7844, October 2007.

[22]   "Simpowersystem Blocks, two-quadrant dc/dc converter," Matlab, 2018. [Online]. Available: https://in.mathworks.com/help/physmod/sps/examples/two-quadrant-dc-dc-converter.html. [Accessed 23 September 2018].

[23]   "OPEC: Annual Statistical Bulletin," Opec.org, 2017. [Online]. Available: http://www.opec.org/opec_web/en/publications/202.htm.. [Accessed 27 October 2017].

[24]   M. P. M. P. Flynn and O. Solis, "Saving energy using flywheels," 2008.

[25]   S. Kim and S. Sul, "Control of rubber tire gantry crane with energy storage based on supercapacitor bank," *IEEE Trans. Power Electron.,* vol. 21, no. 5, pp. 1420-1427, September 2006.

[26]   "Case study: Hybrid rubber tired gantry cranes," Corvus energy, [Online]. Available: https://corvusenergy.com/port-equipment/. [Accessed 19 October 2018].

[27]   *RTG-VSG Hybrid Power Supply System-Operational Manual,* Shenzhen, China: Shenzhen Jingnengfang and System 650 Integration Co., LTD, 2012.

[28]   H. Joon, H. Seung and K. Seung, " Variable-Speed Engine Generator With Supercapacitor: Isolated 699 Power Generation System and Fuel Efficiency," *IEEE Transactions on Industry Applications,* vol. 45, pp. 2130-2135, 2009.